

AD-A121 615

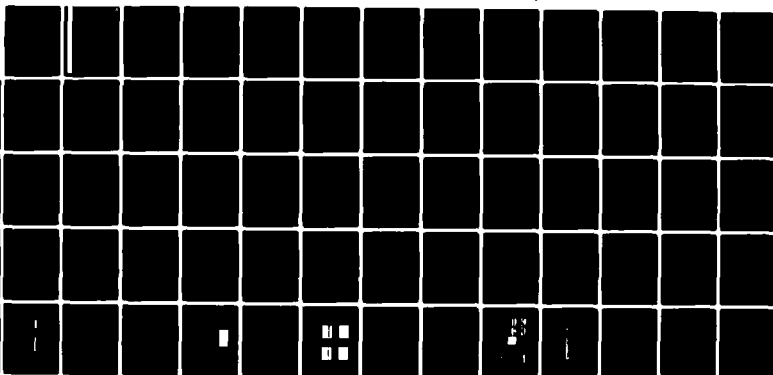
ELECTROSTATIC BURSTS, GENERATED BY ELECTRONS IN LANDAU
RESONANCE WITH WHIS. (U) IOWA UNIV IOWA CITY DEPT OF
PHYSICS AND ASTRONOMY L A REINLEITNER ET AL. JUL 82
U. OF IOWA-B2-24 N00014-76-C-0016

1/1

UNCLASSIFIED

F/G 4/1

NL



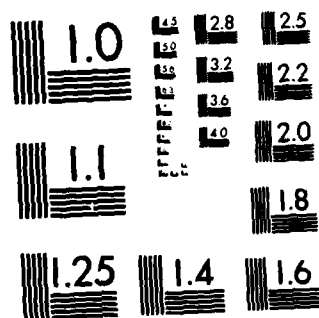
END

DATE

FILED

1-83

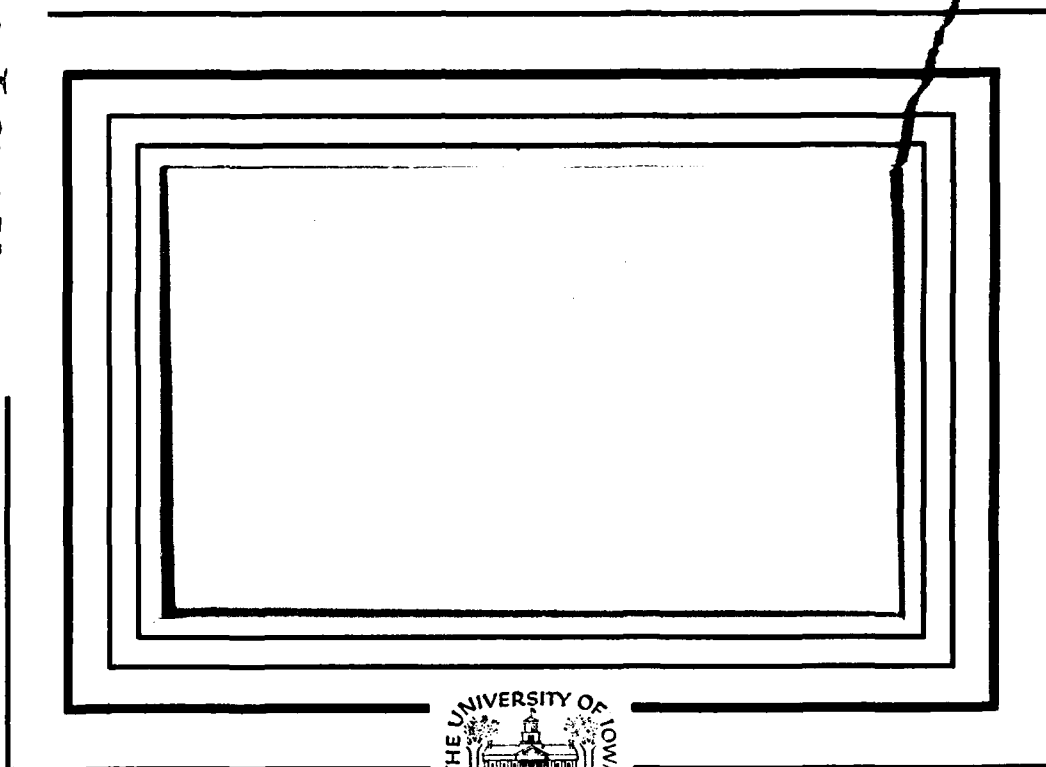
DTIC



MICROCOPY RESOLUTION TEST CHART
NATIONAL BUREAU OF STANDARDS 1963 A

10

AD A121615



DTIC FILE COPY

Department of Physics and Astronomy
THE UNIVERSITY OF IOWA

Iowa City, Iowa 52242

This document has been approved
for public release and sale; its
distribution is unlimited.

DTIC
ELECTE
NOV 19 1982

E

82 11 19 002

U. of Iowa 82-24

ELECTROSTATIC BURSTS GENERATED BY ELECTRONS
IN LANDAU RESONANCE WITH WHISTLER MODE CHORUS

by

Lee A. Reinleitner, Donald A. Gurnett
and Timothy E. Eastman

July, 1982

Department of Physics and Astronomy
The University of Iowa
Iowa City, IA 52242

This research was supported by NASA through grants NGL-16-001-002 and NGL-16-001-043 from NASA headquarters and contracts NAS5-20093, NAS5-26819, and NAS5-11074 with Goddard Space Flight Center, and the Office of Naval Research. The LEPEDEA data reduction from the ISEE 1 instrument was performed through contract NAS5-26257 with Goddard Space Flight Center.

This document is the property of the University of Iowa and is loaned to you for public relations purposes only. No distribution is authorized.

UNCLASSIFIED

SECURITY CLASSIFICATION OF THIS PAGE (When Data Entered)

REPORT DOCUMENTATION PAGE		READ INSTRUCTIONS BEFORE COMPLETING FORM
1. REPORT NUMBER	2. GOVT ACCESSION NO.	3. RECIPIENT'S CATALOG NUMBER
U of Iowa 82-24	AD-A121615	
4. TITLE (and Subtitle)		5. TYPE OF REPORT & PERIOD COVERED
ELECTROSTATIC BURSTS GENERATED BY ELECTRONS IN LANDAU RESONANCE WITH WHISTLER MODE CHORUS		Progress, 1982
7. AUTHOR(s)		6. PERFORMING ORG. REPORT NUMBER
LEE A. REINLEITNER, DONALD A. GURNETT, and TIMOTHY E. EASTMAN		
9. PERFORMING ORGANIZATION NAME AND ADDRESS		8. CONTRACT OR GRANT NUMBER(s)
Department of Physics and Astronomy The University of Iowa Iowa City, IA 52242		N00014-76-0016
11. CONTROLLING OFFICE NAME AND ADDRESS		10. PROGRAM ELEMENT, PROJECT, TASK AREA & WORK UNIT NUMBERS
Office of Naval Research Electronics Program Arlington, VA 22217		
14. MONITORING AGENCY NAME & ADDRESS (if different from Controlling Office)		12. REPORT DATE
		July, 1982
		13. NUMBER OF PAGES
		67
		15. SECURITY CLASS. (of this report)
		UNCLASSIFIED
		15a. DECLASSIFICATION/DOWNGRADING SCHEDULE
16. DISTRIBUTION STATEMENT (of this Report)		
Approved for public release; distribution is unlimited.		
17. DISTRIBUTION STATEMENT (of the abstract entered in Block 20, if different from Report)		
18. SUPPLEMENTARY NOTES		
Submitted to J. G. R.		
19. KEY WORDS (Continue on reverse side if necessary and identify by block number)		
Whistler Mode Chorus Plasma Waves Magnetosphere		
20. ABSTRACT (Continue on reverse side if necessary and identify by block number)		
(See page following)		

DD FORM 1 JAN 73 1473

EDITION OF 1 NOV 65 IS OBSOLETE
S/N 0102-LF-014-6601

UNCLASSIFIED

SECURITY CLASSIFICATION OF THIS PAGE (When Data Entered)



ABSTRACT

Accession For	
NTIS GRA&I	<input checked="" type="checkbox"/>
DTIC TAB	<input type="checkbox"/>
Unannounced	<input type="checkbox"/>
Justification	
By _____	
Distribution/	
Availability Codes	
Dist	Avail and/or Special
A	

Recent studies of wideband plasma wave data from the ISEE-1 and ISEE-2 spacecraft have revealed that whistler mode chorus emissions in the Earth's outer magnetosphere are often accompanied by high frequency bursts of electrostatic waves with a frequency slightly below the electron plasma frequency. Investigations have shown that in some cases the electrostatic waves are modulated at the chorus frequency. Further studies indicate through use of plasma analyzer (LEPEDEA) data on ISEE-1 that these bursts are being produced by a "beam" of electrons in Landau (longitudinal) resonance with the chorus wave and thus moving at the chorus phase velocity. A threshold exists in the chorus intensity below which the electrostatic bursts do not appear.

The high frequency electrostatic waves are believed to be caused by a type of two-stream instability called the resistive-medium instability, produced by electrons trapped by the Landau resonance. A reduction in the electrostatic burst frequency below the electron plasma frequency is a characteristic of the resistive-medium instability. The instability is applicable only in the regime where V_0/V_T is on the order of 1, where V_0 is the velocity of the beam and V_T is the average thermal velocity of the plasma electrons. Our derivation assumes cold ions but warm electrons. The instability requires Landau damping to operate. Thus the beam velocity must be in the region of steep slope on the

electron distribution function rather than in the high velocity tail region. In the cases examined from the LEPEDea data the electron thermal energies are on the order of a few hundred eV. The beam velocities in the observed cases were ≈ 400 eV and ≈ 630 eV, thus verifying that the electrostatic bursts are in the proper regime for the resistive-medium instability.

I. INTRODUCTION

The Earth's magnetosphere has proven to be a rich source of various types of plasma wave modes. This study treats a new type of electrostatic wave that appears as very sharply defined bursts and is closely correlated with a type of electromagnetic whistler mode wave known as chorus. These waves occur in the outer magnetosphere, just inside the magnetospheric boundary layer, on the dayside region of the magnetosphere.

Chorus is a type of low frequency electromagnetic emission that is believed to result from a cyclotron resonance interaction with energetic electrons in the outer magnetosphere. The frequency range of the chorus emissions associated with the electrostatic bursts is approximately 100 Hz to 800 Hz. Chorus usually has a discrete frequency-time structure, consisting of narrowband tones increasing in frequency with increasing time [Helliwell, 1965]. Chorus also occurs as a simple banded emission with little or no structure [Burtis and Helliwell, 1969].

On the dayside of the Earth, chorus waves are generated by electrons with energies in the range of 5 - 150 keV [Burton and Holzer, 1974]. The generation mechanism is believed to be a Doppler-shifted cyclotron resonance with these high energy electrons near the equatorial plane [Dowden, 1962; Brice, 1964; and Helliwell, 1967]. The general resonance condition for a wave of frequency ω interacting with an electron moving in a magnetic field is

$$k_{\parallel} v_{\parallel} = \omega - m|\omega_{ge}| \quad (1)$$

where $m = 0, 1, 2, \dots$ are integers, v_{\parallel} and k_{\parallel} are velocity and wave vector components parallel to the magnetic field, and ω_{ge} is the electron gyrofrequency.

For cyclotron resonance, the integer m must be nonzero. The special case where m is zero is called the Landau resonance. Kennel and Petschek [1966] showed that the whistler mode is unstable if a positive pitch angle anisotropy exists in the electron distribution function at the resonance velocity. In the Earth's magnetosphere a positive pitch angle anisotropy is produced by a loss cone in the trapped electron distribution. Electrons resonating with the wave are always scattered toward the loss cone by the cyclotron resonance interaction, thereby causing the particles to be precipitated into the atmosphere. Precipitating electrons have been reported in association with chorus emissions [Oliven and Gurnett, 1968; Rosenberg et al., 1971] and are believed to be pitch angle scattered by these waves.

Chorus has been known for many years [Helliwell, 1965] to be propagating in the whistler mode. For the parameters found in this study, the chorus phase velocity was typically on the order of 1/10 to 1/20 of the speed of light. Although the ray path of the chorus wave tends to follow the ambient field line, the wave vector can be at a substantial angle θ to the field line [Kennel and Thorne, 1967; Burton and Holzer, 1974; Burtis and Helliwell, 1976]. The general magnitude of θ is still a subject of some debate due to the lack of wave normal measurements,

but is generally believed to be in the range from about 0° to 30° [B. T. Tsurutani, private communication, 1982].

→ The electrostatic bursts analyzed in this paper have a frequency much greater than that of the chorus. The frequency is usually somewhat lower than the electron plasma frequency and is normally in the range from about 3 kHz up to 10 kHz. As will be shown, the electrostatic bursts are longitudinal electrostatic waves with wave vectors aligned almost exactly along the ambient magnetic field. In some cases, the amplitude of the electrostatic bursts is shown to have a modulation at the chorus frequency. This modulation is indicative of a strong physical interaction between these two wave modes.

This paper details the investigation of this interaction and provides strong evidence that the electrons responsible for the electrostatic bursts are trapped and accelerated by a Landau resonance interaction with the chorus wave. The primary data used in this work was obtained from the ISEE 1 and ISEE 2 (International Sun-Earth Explorer) spacecraft, which were launched into Earth orbit simultaneously on October 22, 1977. A description of the spacecraft orbital parameters is contained in Anderson et al. [1981]. The plasma wave data used was obtained from the University of Iowa Plasma Wave Experiment, and the instrumentation is described in detail by Gurnett et al. [1978]. All of the electric field data taken on the ISEE 1 spacecraft for this work used the 215 m electric dipole antenna. The electric dipole antenna on ISEE 2 has a length of 30 m tip-to-tip.

High time resolution spectrum measurements were available on ISEE 1 from a 20-channel electric spectrum analyzer which covered a range from

5.62 Hz to 311 kHz, as well as extensive frequency time measurement using the wideband instrumentation. The wideband receiver was used in a mode with two frequency channels for all of this work. One channel extended from 650 Hz to 10 kHz and was transmitted by directly modulating the wideband transmitter output. The other channel extended from 10 Hz to 1 kHz and was transmitted using an FM subcarrier. Due to the large dynamic range the wideband receiver was provided with an Automatic Gain Control (AGC) which maintained a nearly constant signal amplitude.

Valuable data on the electron velocity distribution function were obtained from the University of Iowa Quadrispherical LEPDEA (Low Energy Proton and Electron Differential Energy Analyzer) instrument. Full descriptions of the LEPDEA instrument are given by Frank et al. [1978a,b]. The LEPDEA instrument samples ion and electron velocity distributions over approximately 98% of the unit sphere. This coverage is obtained by seven pairs of sensors which are used to segment the 162° polar angle range into seven contiguous fields-of-view. One of the primary LEPDEA data formats is in the form of E- ϕ spectrograms. This data format is explained in detail in Eastman and Frank [1982].

II. CHARACTERISTICS OF THE ELECTROSTATIC BURSTS AND THEIR RELATIONSHIP TO WHISTLER MODE CHORUS

This section is devoted to a description of the electrostatic bursts observed and their relationship to the whistler mode chorus emissions accompanying them. A preliminary study of these relationships has been published by Reinleitner et al. [1982]. Figure 1 indicates some of the general features of this phenomenon. The top panel shows a chorus band at about 150 - 200 Hz, of the type that is often observed in the outer magnetosphere on the dayside of the Earth. The frequency is somewhat lower than the chorus frequencies usually reported in the literature due to the low magnetic field strength in the outer part of the magnetosphere. The discrete features in Figure 1 are a general class of emissions called "hooks" by Helliwell [1965]. In this case the emissions only have rising frequencies, but hook-like features with both descending and then rising frequencies are often observed [Reinleitner et al., 1982].

The features referred to as electrostatic bursts (or simply bursts) are illustrated in the lower panel of Figure 1. These bursts extend in a fairly broad band from about 3 kHz to about 7 kHz and turn on and off very abruptly (on the order of ten milliseconds). In this case, the electrostatic bursts appear to be strongly correlated to discrete features in the chorus band.

Two particular types of electrostatic bursts occur, both related to chorus. The first type is shown in Figure 1 where the bursts are of short duration, usually less than one second. This type of burst is usually correlated to a hook-like feature in the chorus band. The second type is of longer duration and is associated with an intensification of the chorus band rather than a hook-like feature. This type of burst is illustrated in Figure 2. The intensification of the chorus band in this figure is a real feature as determined by the spectrum analyzer data and not simply a AGC effect. The rather abrupt onset and termination of the electrostatic bursts in association with the chorus band intensification indicates that some type of threshold effect is present. Long duration bursts are observed to extend from about 10 seconds to several minutes. The long duration type of electrostatic bursts are much more commonly observed than the type associated with the discrete hook-like features by roughly a factor of 5 to 10.

A comprehensive survey of the locations where the bursts can be observed has not yet been performed. However, all cases observed so far have been located in the Earth's outer magnetosphere near the dayside magnetospheric boundary at about 9 - 12 R_E . Cases have been found on the dayside region for magnetic local times ranging from 7.0 to 17.5 MLT. All cases observed have been within 30° of the magnetic equator; however, this limitation is probably due to the equatorial nature of the ISEE satellite orbit. Examination of the LEPEDEA data has shown that most of the observed cases are located inward from the magnetospheric boundary layer. Only a few are actually located in the boundary

layer region itself. It should be noted that in regions closer to the Earth, the plasma frequency tends to go above 10 kHz, which would produce electrostatic bursts at frequencies too high to be observed in the primary mode of operation of the ISEE instrumentation. Thus the general limitations on the locations of the observed electrostatic bursts accompanied by chorus should be viewed partly as an instrumental limitation rather than a definitive region of occurrence.

The frequency of the bursts have always been observed to be below the local plasma frequency (f_p), as determined by the lower edge of the continuum radiation [Gurnett and Shaw, 1973]. This difference between the emission frequency and the plasma frequency varies from essentially undetectable, to as much as 60 percent. The burst frequency was always well above the local electron gyrofrequency as determined by the magnetometer data [Russell, 1978]. The bursts always occur in a broad frequency band, as opposed to a sharp monochromatic emission. The bandwidth is usually a few hundred Hz to several kHz.

The bursts have been described as electrostatic because no wave magnetic field has been detected in association with them. Typically the broadband electric field strength of the bursts is on the order of 50 $\mu\text{V/m}$. Because the wave magnetic field remains at the instrument noise level in all cases observed, a limit can be placed on the magnetic-to-electric field ratio of about $cB/E \lesssim 4$, which corresponds an index of refraction $n \lesssim 4$. Because no electromagnetic plasma wave mode is known to exist with $cB/E \lesssim 4$ in the frequency range $f_g < f_{\text{burst}} < f_p$, the bursts are almost certainly electrostatic. The typical

electric and magnetic field strengths of the chorus emissions associated with the electrostatic bursts are about 300 $\mu\text{V/m}$ and 40 nT, respectively.

Serious consideration was given to the possibility that the electrostatic bursts are an instrumental effect. For reasons outlined in Reinleitner et al. [1982], which included observations of the electrostatic bursts on IMP 6 data, we have concluded that the bursts are not an instrumental effect. In addition, the good correlation with LEPDEA electron data shown in Section IV also indicates that the electrostatic bursts accompanying the chorus are not due to an instrumental effect.

The electrostatic bursts occasionally have narrowband harmonic structure as shown in Reinleitner et al. [1982]. The frequency spacing of the harmonic structure corresponds to the instantaneous emission frequency of the chorus burst. This feature will be discussed again later in this section.

When chorus hooks are found to be correlated with the electrostatic bursts, the onset of the electrostatic burst usually coincides with the minimum frequency of the hook. This effect may be due to the chorus having the greatest intensity at about the minimum in the hook feature, or due to the rising frequency of the hook after the minimum. It should be noted that the electrostatic burst often continues for a time after the hook has disappeared or merged back into the chorus band.

To identify the mode of propagation of the electrostatic bursts it is useful to try to determine the wavelength and polarization of these waves. The different antenna lengths on ISEE 1 and ISEE 2 have been used to determine the wavelength limits of the bursts. Figure 3 shows an example of the electric field spectra obtained simultaneously for a

long burst that was observed in the wideband data by both ISEE 1 and ISEE 2. These spectrums indicate, when corrected for the antenna length of each spacecraft, that the electric field strength for both the chorus and the electrostatic bursts is the same at both spacecraft even with different antenna lengths. The fact that the electrostatic burst shows the same electric field strength independent of the antenna length indicates that the wavelength of the burst must also be greater than the length of either antenna [Gurnett and Frank, 1978]. Thus the wavelength of the electrostatic bursts must be longer than the ISEE 1 electric dipole antenna, so that $\lambda_{\text{burst}} > 215$ meters.

Further studies of the wideband data show that although there is a good correlation between chorus hooks in both ISEE 1 and ISEE 2 data, the detailed correlation between the electrostatic bursts is relatively poor. A strong correlation does exist between the overall occurrence of bursts, which is probably due to the correlation between the bursts and the chorus itself. However, a good correlation does not exist between the structure of the individual elements of the bursts at the two satellite locations. This indicates that the wavelength of the bursts is shorter than the distance between the two spacecraft. Thus we can say that $215 \text{ m} \lesssim \lambda_{\text{burst}} \lesssim 100 \text{ km}$.

The rapid sample data has been used to determine the polarization of the electrostatic bursts. In a case where the channel of the multi-channel electric spectrum analyzer on ISEE 1 was set at about the frequency of the electrostatic burst and was also in the rapid sample mode, it is possible to determine the polarization from the spin

modulation of the electric field intensity. An example of this type of polarization analysis is shown in Figure 4 which shows that the electric field of the bursts appears to be aligned with the projection of the ambient magnetic field in the spin plane of the spacecraft. This result indicates that the electrostatic bursts have a wave vector (\vec{k}) generally aligned along the ambient magnetic field. It should be noted here that, even though the long bursts in the wideband data do not show a spin modulation effect because of the AGC, several checks of the spectrum analyzer data show that the spin modulation is present.

Since the wideband data is transmitted from the satellite in analog form and is spectrum analyzed on the ground, it is possible to study the actual waveform as seen by the electric field antenna on the spacecraft. An example is shown in Figure 5. The electric field versus time waveform for both the chorus and electrostatic burst is shown in the lower panel for the very short burst marked in the middle panel at 1739:23 UT. The lower signal is the chorus waveform while the upper high frequency signal is associated electrostatic burst waveform. Both signals have been processed by bandpass filters to eliminate signals not in the frequency band of interest. As can be seen, the electrostatic noise is actually composed of many shorter bursts of a high frequency signal which is modulated at the chorus frequency. Thus, the harmonics mentioned earlier are a modulation effect caused by the periodic modulation of the electrostatic noise at the frequency of the chorus emission. In the cases where harmonics are not observed, the electrostatic burst occurs in a broad frequency band which tends to blend any harmonics into a broad continuous spectrum. It is also noted that for the long electrostatic bursts, the modulation effect is either not as strong or nonexistent. This effect is

illustrated in Figures 6A and 6B, which show an example of a good modulation effect on a short burst associated with a hook. In Figures 6C and 6D a longer burst of about 6 seconds duration shows a much reduced modulation effect. Due to possible phase shift effects in the filters used for the waveform analysis and other unknown phase shifts related to the wave normal angle, nothing can be said at this point about the absolute phase relationship between the chorus waveform and the modulation of the electrostatic burst.

To summarize the characteristics covered in this section, we have noted that electrostatic bursts appear to accompany chorus "hooks" and simple chorus intensifications in the Earth's outer magnetosphere. These bursts seem to have a wavelength such that $215 \text{ m} \lesssim \lambda_{\text{burst}} \lesssim 100 \text{ km}$. The electric field vector of the electrostatic bursts is aligned along the ambient magnetic field, and thus the wave vector is also aligned along the magnetic field. Examination of the waveforms for both the chorus and bursts indicate that often the higher frequency waveform for the burst is modulated by the chorus waveform. The strong correlation between the envelope of the electrostatic bursts and the chorus suggests some strong physical interaction between these two wave modes.

III. MODEL INTERPRETATION OF OBSERVATIONAL DATA

In the previous section, the observations of the electrostatic bursts accompanied by whistler mode chorus were described. This section describes a model that explains the observations. The most obvious characteristic of the bursts is that they are electrostatic and near the electron plasma frequency. This could suggest some form of Langmuir oscillation. However, the fact that the emission frequency occurs below the electron plasma frequency requires some explanation because the Langmuir oscillation always occurs at frequencies near or slightly above the electron plasma frequency. Parametric interactions between the electrostatic mode and the chorus are considered unlikely because the electrostatic bursts sometimes last longer than the chorus burst. Because the wave vector for the bursts is apparently aligned in the general direction of the ambient magnetic field, the observations suggest a two-stream instability with a field-aligned beam.

The general model that is proposed is illustrated in Figure 7. It is well known that whistler mode chorus in the magnetosphere has a wave normal vector that is typically at an oblique angle to the magnetic field [Burton and Holzer, 1974]. The top part of Figure 7 shows that when the wave normal angle θ is non-zero, the electric field of the chorus wave has an electric field component \vec{E}_1 along the \vec{B}_0 field. Because the ambient magnetic field \vec{B}_0 in the region of interest is on

the order of 40 nT, and the wave magnetic field of the chorus is on the order of 40 pT, it is expected that the first order motion of the electrons will be the usual helical motion along the ambient magnetic field line.

The model, as proposed, assumes that the electrons are free to move along the ambient magnetic field line (\vec{B}_0), under the influence of the parallel electric field (\vec{E}_{\parallel}) of the chorus wave. Thus the electrons will only be affected by an effective potential due to \vec{E}_{\parallel} such as that shown in the middle part of Figure 7. This electric field permits electrons to be trapped in effective potential wells of the chorus wave and to be carried along with the chorus wave at the chorus phase velocity.

These trapped electrons will move in bunches at the chorus phase velocity in the effective potential wells and, to a stationary observer, would pass by in a periodic manner with the chorus wave. Because the trapped electrons move at the same velocity, these electrons effectively have a delta function velocity distribution and would therefore be expected to excite Langmuir waves via a two-stream like mechanism. The bursts of Langmuir waves would then be expected to have the modulated characteristics of the short electrostatic bursts as shown in the bottom part of Figure 7.

For the plasma parameters in the region of interest, the index of refraction for the whistler mode is on the order of 10 to 20. This implies a phase velocity of somewhat less than one tenth the velocity of light. From the wavelength and electric field intensity of the chorus wave it is possible to estimate the depth of any possible potential

well. A simple calculation (assuming $n = 10$ and $f = 300$ Hz) gives:
 $\lambda = V_p/f = 100$ km. This wavelength implies that for a chorus wave with an electric field intensity of about $300 \mu\text{V/m}$, such as reported in Section II, the potential well would be $100 \text{ km} \times 300 \mu\text{V/m} = 30$ volts. This value is encouraging, as it is large enough to be a significant potential for electrons with energies of a few keV. With an index of refraction of about 10 or 20, the electrons moving at the chorus phase velocity will have an energy of ≈ 2 keV or less.

Early work on resonances by Kennel and Petchek [1966] concentrated on studies of electron cyclotron resonance interactions ($m = 1, 2, \dots$ in Equation 1). The possibility of particle trapping by Landau resonance interactions ($m = 0$ in Equation 1) with chorus waves has only recently been considered. Nunn [1971; 1973] investigated the trapping of particles by Landau resonant interactions with electrostatic waves. A more recent work by Inan and Tkalcevic [1982] deals with the nonlinear equations of motion for particles in Landau resonance with chorus waves. The work of Inan and Tkalcevic [1982] is greatly extended in a Doctoral Dissertation by S. Tkalcevic [1982] in which the Landau resonant trapping properties of whistler mode waves are explored. His computer model simulations yield several important new results and conclusions, including the finding that an intensity threshold exists, below which trapping is not possible. This threshold depends on several parameters, most notably the wave vector angle θ from the \vec{B}_0 field, and is in general on the order of $E_{0\parallel} \approx 20 \mu\text{V/m}$. In all cases of the observation of electrostatic bursts, the chorus intensity was well above this threshold, usually on the order of $E_0 \approx 300 \mu\text{V/m}$.

To demonstrate the trapping of electrons at the Landau resonance for the specific parameters relevant to this study, a computer simulation was performed by solving for the motion of an electron in the presence of a whistler mode wave propagating at an angle to the \vec{B}_0 field. Using the cold plasma dispersion relation given by Stix [1962], equations for the electric and magnetic field components of a whistler mode wave can be obtained [Reinleitner, 1982]. The computer model uses a box with the z-axis along the \vec{k} vector of the wave and a length of one wavelength. This models gives periodic boundary conditions on the box where the x and y lengths are arbitrary. The electric and magnetic fields in the box are thus only functions of the z-axis position and time. The electron is injected at a velocity slightly greater than the wave phase velocity projected along the ambient magnetic field, and the wave intensity is allowed to grow linearly with time. The fourth order Runge-Kutta method is used to solve the first order equations for the acceleration and position as a function of time. The time step is about one-twentieth of the electron cyclotron period.

The results for three different wave vector angles θ are shown in Figure 8. The parameters used are $\omega = 1885 \text{ sec}^{-1}$, $n_e = 1.0 \text{ cm}^{-3}$ and $B_0 = 40 \text{ nT}$, which are typical for the events illustrated in Figures 1 and 2. Trapping occurs when the whistler mode intensity exceeds a threshold intensity. In this illustration $V_p/\cos \theta$ is the projected wave phase velocity along the ambient magnetic field (\vec{B}_0), V_z is the initial particle velocity along \vec{B}_0 , and ΔE is the energy difference between an electron moving at $V_p/\cos \theta$ and one moving at V_z . Z-phase is the relative phase between the electron position and the wave front. Trapping

is defined as the point in time when the phase variation of z -phase becomes bounded. Trapping occurs when the electric field amplitude E_0 becomes large enough to produce bounded oscillatory motion (on the order of $40 - 80 \mu\text{V/m}$). The results obtained show that the required E_0 for trapping decreases as the wave vector angle θ increases. These computer simulations show that particle trapping occurs at electric field intensities that are consistent with those found in Tkalcevic [1982].

Electrons may be trapped in the potential well of the chorus wave by at least two possible mechanisms. In the first mechanism the chorus wave amplitude simply increases with time due to the loss-cone instability, thereby trapping electrons with velocities close to the chorus phase velocity, as was done in the particle simulation described. In the second mechanism the chorus phase velocity increases, and trapping occurs when the phase velocity matches the velocity of some of the electrons in the high energy tail of the thermal electron distribution.

Electrons may also be detrapped by several possible mechanisms. Mutual electrostatic repulsion due to too many trapped electrons could push some of the electrons out of the potential well (Poisson's equation is neglected for the simulation). The chorus wave may accelerate in phase velocity at so great a rate as to dump or "slosh" electrons out of the potential wells. Furthermore, as the wave propagates into regions of stronger magnetic field, the magnetic moment force, $-\mu\partial B/\partial z$, can become large enough to detrapp the electrons.

Trapping alone would probably not explain enough electron enhancement at the chorus phase velocity to create a two-stream bump-on-tail instability, since trapped electrons oscillating in the potential well

still have the same range of velocity as before trapping occurs. Some mechanism is required to translate these electrons into a region of velocity space with a lower phase space density so that a double-humped velocity distribution is produced. A likely candidate is some form of acceleration in which the chorus first traps the electrons as the wave grows in amplitude, and then accelerates the trapped electrons. This process is illustrated in Figure 9, where a chorus wave generated at the equator propagates along the magnetic field line to higher latitudes. As the wave packet moves to higher latitudes, the magnetic field strength increases, thereby increasing the phase velocity and accelerating any electrons that were trapped by the wave. The increase in the magnetic field strength is, of course, in competition with the increasing plasma density at higher latitudes which would tend to increase the index of refraction. Because of the high electron temperature in the region, it is not clear which trend would dominate. Another possible acceleration mechanism is suggested by the hooks, such as those in Figure 5. The electrostatic burst usually seems to be associated with the rising portion of the hook. As the frequency of the hook rises, the index of refraction decreases, thereby increasing the phase velocity. This frequency variation can accelerate electrons trapped in the wave packet to higher velocities.

The exact method of electron acceleration to create a positive slope in the distribution function has not been clearly established. Some gain in velocity for certain electrons, however, is required for the model. The effect of this electron acceleration is to move part of

the distribution function up to higher velocities, thereby creating a bump in the new distribution function as illustrated in Figure 9. Only a small increase in velocity would be necessary for a two-stream instability to arise if the trapped electrons have a sufficiently narrow velocity spread.

IV. ELECTRON DISTRIBUTION FUNCTIONS

The most obvious feature predicted by the model described in Section III is the existence of the enhanced trapped electrons which should be moving at the phase velocity of the chorus wave. Knowing the plasma frequency from the cutoff of the continuum radiation, the 64 sec averaged magnetic field from the Data Pool tape, and the chorus frequency as obtained from the wideband data, it is possible to determine the phase velocity of the whistler mode wave. The only unknown parameter is the wave normal angle θ . The phase velocity is, however, only weakly dependent upon θ , unless θ is quite large. Using the theoretical value of the phase velocity, a search for an electron beam aligned along the \vec{B}_0 field was performed using the LEPEDea instrument on ISEE 1.

Several difficulties arise in using particle data to search for this electron beam. The main limitation in the LEPEDea instrument for this purpose is the time required for a full energy scan. An entire three dimensional distribution function requires about 2 minutes (128 seconds) when the satellite is in the high bit rate mode, while most electrostatic bursts are much shorter than a two minute duration. Short bursts accompanying chorus hooks may often not be observed with the LEPEDea data. A careful study was made of the ISEE 1 wideband data to find cases where the electrostatic burst was long enough for an efficient study of the LEPEDea data. Ten possibilities were found where either one long electrostatic burst or several shorter electrostatic bursts covered at least 70% of a two-minute period in the wideband data.

These possibilities were checked with detailed computer listings of the LEPEDea instrument responses. We anticipated that a beam would not be detected in some of these cases due to several factors. Since only a few energy scans from the full 128 second energy cycle will be at the correct energy to detect the beam, there is a high probability that the burst would not be occurring at the appropriate sample time. In addition, the plasma density in the outer magnetosphere is usually very low, typically less than $1 \text{ electron cm}^{-3}$, so that plasma analyzers often obtain relatively low responses in this region. Out of the ten selected cases, three showed no clear sign of any beam-like enhancement, and seven showed some detection of an electron enhancement. This enhancement is referred to as a beam in this paper, though careful examination shows that it may not correspond to an idealized delta function beam. Due to limitations of computer time only the two best cases in the instrument response listings were analyzed in detail.

In the $E-\phi$ spectrogram of Figure 10 detectors 2E and 6E are the detectors that point along the ambient magnetic field line as determined from the orientation of the spacecraft and the magnetic field data from the magnetometer experiment [Russell, 1978]. The horizontal axis in each spectrogram is the rotational angle ϕ of the spacecraft and the vertical axis is the particle energy (P for protons and E for electrons). The magnetometer data shows that features labeled "field-aligned enhancements" occur when the detector is pointing along the magnetic field. Thus, the enhancements are field-aligned which is the expected direction for a beam in Landau resonance with the chorus.

One clear feature that emerges from Figure 10 is that there are actually two counterstreaming electron enhancements at the same energy. This effect is easily understood if the bounce time for a mirroring particle is examined. From Van Allen [1961], an equation for the bounce time of an electron trapped in the Earth's geomagnetic field is given by:

$$\tau_2 = 0.85(r_0/\beta) T(\alpha_0) \text{ seconds} \quad (9)$$

In this equation r_0 is the equatorial radial distance in Earth radii, β is v/c , and $T(\alpha_0)$ is a parameter ranging from about 0.56 to 1.3. Thus the bounce period for $r_0 \approx 10 R_E$, $\beta \approx 1/10$, and $T(\alpha_0) \approx 1$ is $\tau_2 = 8.5$ seconds. This estimate shows that the bounce period is on the order of 10 seconds. Thus for long bursts, such as the ones examined in this study, the electrons will be mirroring back and forth along the field line and will show up in the LEPEDea data as a symmetric field-aligned distribution.

It is also worth noting here that the LEPEDea instrument is not expected to temporally resolve the modulated or periodic nature of the electron enhancements. The instrument averages over a 0.25 second sample interval. It is expected that for the long bursts, the spatial bunching of the electrons is no longer occurring. In the waveform studies of the long bursts, the modulation effect is not very dominant and is often completely absent. A very strong possibility exists that any electron trapping and acceleration may be occurring at some other location along the field line, and that the electron enhancements

observed by LEPDEA instrumentation are no longer moving at the local chorus phase velocity.

For the case in Figure 10, on day 222/79, the following plasma characteristics were noted: $f_p \approx 5.7$ kHz, $f_{\text{chorus}} \approx 150$ Hz and $B_0 = 25.1$ nT. These parameters yielded a value for the index of refraction of 19.8, which would correspond to an electron moving with an energy of 650 eV ($\pm 40\%$), while the center of the enhancement in Figure 10 is at 630 eV ($\pm 20\%$). This close agreement should be regarded as somewhat fortuitious, since for the second case on day 263/80, the agreement is less exact. The plasma parameters for the second case are: $f_p \approx 6.5$ kHz, $f_{\text{chorus}} \approx 400$ Hz, and $B_0 = 30.8$ nT. These parameters yield a value for the index of refraction of 15.1, which would correspond to an electron moving with an energy of 1120 eV ($\pm 30\%$), while the center of the enhancement was at 400 eV ($\pm 20\%$). Because the local chorus phase velocity and the beam velocity differ by a significant amount ($V \propto \sqrt{\text{Energy}}$), the acceleration of the ≈ 400 eV electrons is probably taking place somewhere else along the magnetic field line. In this case, the beam electrons may have been accelerated by a change in the chorus phase velocity before escaping from the potential well through one of the mechanisms described in Section III.

In both of the cases examined the electron enhancements were found to occur in the E- ϕ spectrograms when the long duration burst appeared, and to persist for several minutes afterward, fading out gradually, rather than abruptly turning off as the electrostatic burst does. The case of day 263/80 is shown in Figure 11. The upper portion of Figure 11 shows a standard case of wideband data from ISEE 1 For September 19-20, 1980. In this figure the chorus shows up clearly as a dark band in

the upper panel at about 300 Hz. The electrostatic burst shows up as a dark band in the lower panel from about 3.5 - 7.0 kHz. The fact that the continuum radiation from about 6.5 - 10 kHz ceases when the electrostatic burst appears is caused by the AGC, because the burst is of much greater intensity than the continuum radiation. The time scale is much longer than other wideband figures in this work. It covers a period of 10 minutes with the 2.5 minute electrostatic burst labeled at its start time with an S, and its end time with a T. There is a long period after the end of the burst with little or no chorus and burst activity.

The lower portion of Figure 11 shows a time series of E- ϕ spectrogram panels for the same time period. Only detectors 2E and 6E are important in this time period as they show the field-aligned electron beams very clearly. These beams are also aligned along the ambient magnetic field. Time as well as energy is given on the ordinate of each detector panel with a time of ≈ 128 seconds per panel. The start times of each panel are given between the corresponding detector panels. The start time of the burst is indicated by S, and the end time by a T. As can be seen, the field-aligned electron enhancement is strongest during the burst, and gradually fades away. A clear relationship is evident in this data between the simultaneously occurring chorus and burst, and the field-aligned electron enhancements or "beams". The gradual fading out of the beams after the end of the electrostatic bursts may be accounted for by the the mirroring electrons bouncing back and forth between their conjugate mirror points several times before being lost.

A perspective plot showing the entire electron distribution function for a two-minute interval on day 222 in 1979 is shown in Figure 12. This plot corresponds to the event shown in Figure 10. The perspective plot clearly shows the field-aligned enhancements. By integrating over just the enhancement and subtracting the distribution without the enhancement, a value for the beam density can be obtained. The value of the beam density divided by the plasma density is 2.5×10^{-3} for the positive v_{\parallel} enhancement, and 1.3×10^{-3} for the negative v_{\parallel} enhancement. If a cold electron component exists that is not detected by the LEPEDea instrument, then these values would have to be lowered slightly. From the plasma density values estimated from the continuum radiation cutoff in the wideband data, these values would have to be lowered by about a factor of two. The field-aligned electron enhancements are therefore about three orders of magnitude less than the ambient plasma density.

If an energy gain of about 30 eV is assumed for each electron in the enhancement, and the chorus wave is assumed to have a magnetic field intensity of approximately 40 pT, the wave energy density of the chorus is approximately the same as the energy gain per unit volume for the electron enhancement. Most of the chorus wave energy resides in the magnetic field. Thus, the chorus wave energy appears to be adequate to create the electron beam. The electric field energy density of the electrostatic burst is about three orders of magnitude less than the energy density of the chorus wave if the value of 50 $\mu\text{V/m}$ is used. Thus, energy considerations for the model outlined in Section III would appear to be satisfied.

V. THE THEORY OF THE RESISTIVE-MEDIUM INSTABILITY AND ITS COMPARISON TO OBSERVATIONS

The standard two-stream theory, as described in most introductory plasma physics texts such as Krall and Trivelpiece [1973], is not adequate to describe the observations of the electrostatic bursts. The primary difficulty is that for a simple bump-on-tail distribution function the frequency of maximum growth rate is predicted to be near or slightly above the electron plasma frequency, $\omega^2 = \omega_{pe}^2 + 3\langle v_z^2 \rangle k^2$, whereas the bursts usually occur below the electron plasma frequency.

This difficulty is improved slightly if a finite beam density is considered, as in Equations 1.51 and 1.52 from Mikhailovskii [1970]. Mikhailovskii's derivation assumes a finite but small beam density represented by the parameter $\alpha \ll 1$ where $\alpha = n_b/n_e$, n_b is the beam density, and n_e is the plasma electron density. Using a simple Taylor expansion about ω_{pe} , the first order corrections to the dispersion relation can be obtained with the result that the frequency and growth rate are given by

$$\text{Re } \omega = \omega_{pe} \left[1 - \frac{\alpha}{(2)^{4/3}} \right]^{1/3} \quad (2)$$

and

$$\text{Im } \omega = \omega_{pe} \frac{\sqrt{3}}{(2)^{4/3}} \alpha^{1/3} \quad (3)$$

This finite beam approximation provides a reasonable growth rate for the instability, and a reduction in the frequency of the oscillation below the plasma frequency. The reduction in the frequency below the plasma frequency is, however, not sufficient to explain the large (60%) reductions sometimes observed for the electrostatic bursts unless a totally unreasonable beam density is assumed ($\alpha \approx 1$). Such a large beam density would likewise invalidate the assumption that $\alpha \ll 1$. In Section IV, we found that the LEPEDA data yielded $\alpha \approx 10^{-3}$.

A different type of instability that explains many of the above difficulties is discussed in Briggs [1964]. This instability is called the resistive-medium instability. The derivation of this instability is outlined in Appendix A. This derivation is made for a one-dimensional system. It assumes a weak beam system with the beam and the background plasma ions being cold but with the background electrons being warm. In this derivation, a resonance distribution was used for the background electrons for mathematical simplicity. The derivation in fact shows two types of instabilities, called the reactive-medium instability and the resistive-medium instability, both of which are important under different regimes of V_0/V_T , where V_0 is the "beam" velocity and V_T is the r.m.s. thermal velocity.

The reactive-medium instability has a large growth rate when $V_0 \gg V_T$ and is essentially the normal bump-on-tail two-stream instability, yielding results virtually identical to Equations 12 and 13. The resistive-medium instability is a different type of instability which requires dissipation and occurs when V_0 is on the order of V_T . This

condition means that Landau damping is essential to the instability and that the beam must be on the slope of the distribution, not on the tail. The resistive-medium instability only occur for very low velocity beams, or plasmas with very hot electrons. This latter case applies to the outer magnetosphere. As given in Section III, the thermal velocity in the regions of interest corresponds to electron energies in the range of 200 - 600 eV. Thus for electron beams with energies from 200 eV to 2 keV, we are well in the range of the resistive-medium instability.

With the use of Equations 7, 8, and 9 derived in Appendix A, a plot can be made of the imaginary component of ω versus the real part of ω . The entire imaginary component of ω is contained in $\delta\omega$ and, from Equation A7, it is seen that the imaginary part is always multiplied by ω_{pb} , the plasma frequency due to the beam alone. Thus the growth rate is directly related to the beam density. Figure 13 shows the growth rate as a function of the frequency where ω_i is scaled by ω_{pb} , and the real frequency is scaled by ω_{pe} . Several cases of V_0/V_T are shown. From this illustration it is very clearly seen that for cases where V_0/V_T is close to 1, there is a very significant downshift in the frequency of maximum growth rate below the electron plasma frequency. This downshift below ω_{pe} is easier to understand from Figure 14 in which the frequency of maximum growth is plotted versus V_0/V_T . Since the electron beams actually observed have energies of 400 eV and 630 eV, and the thermal velocity in the outer magnetosphere corresponds to electron energies in the range of $\approx 200 - 600$ eV, it is seen from this figure that the downshift in frequency below the plasma frequency can vary from a few percent to sixty percent, in agreement with observations.

The absolute growth rates predicted by the theory must match the growth rates shown in Figures 5 and 6 for the burst waveforms. If $\omega_1 = 1/\tau$ where τ is the time required for the envelope of a modulated burst to increase by a factor of e , then to an order of magnitude from the theory as graphed in Figure 13: $\omega_1/\omega_{pb} \approx 1$. From the waveforms in Figures 5 and 6 we also observe that: $\omega_1/\omega_{pe} \approx 3 \times 10^{-2}$. These experimental values lead to the conclusion that $\omega_{pb}/\omega_{pe} \approx 3 \times 10^{-2}$, which implies that:

$$\alpha = \frac{n_b}{n_e} \approx \left(\frac{\omega_{pb}}{\omega_{pe}} \right)^2 \approx 10^{-3} \quad .$$

This value, predicted from the theory and the experimentally determined growth rate, indicates that the beam density should be about three orders of magnitude less than the plasma density, which is in agreement with the LEPDEA results. Thus, the absolute growth rate predicted by the theory is of the correct magnitude as compared to the observed growth rates and the LEPDEA beam density results.

Another important factor is noted in the curves of Figure 13. As V_0/V_T decreases, the peak in the growth curves becomes narrower. This observation predicts a tendency that had not initially been noticed in the wideband data. There is a tendency for cases of electrostatic bursts that are downshifted in frequency by a large percentage of f_p to have a wider spread in the frequency band excited. This tendency is illustrated in Figure 15 which shows a large number of cases where the spread in the observed frequencies divided by the center of the burst

frequency is plotted versus the center of the burst frequency divided by the plasma frequency. Figure 15 indicates that a clear correlation exists between these two observed characteristics of the electrostatic bursts.

In order to obtain some idea what the theoretical relationship between these two parameters should be, an examination is made of the range of growth rates expected to be observed in the wideband data. The range in intensity observable in the wideband data is better than 10dB. If one assumes that the amplitude of the burst at a particular frequency is dependent on the imaginary component of ω at that frequency, then spread of frequencies observed in the wideband spectrograms will be those frequencies that have an amplitude within 10 dB of the central frequency of maximum amplitude. Estimates show that the reduction in the growth rate ω_i that is visible in the wideband data, to that growth rate ω_i that is just barely detectable in the wideband data, is a constant factor [Reinleitner, 1982]. Taking a case from Figure 13 where $\omega/\omega_{pe} = 0.85$, we observe from Figure 15 that the corresponding frequency spread is $f_s/f_b \approx 0.3$. In Figure 13 a dotted line indicating $f_s/f_b \approx 0.3$ (where f_s is the frequency spread of the burst, and f_b is the center frequency of the burst) is drawn on the ω_i curve for $V_o/V_T = 4.0$. Using the same ω_i reduction for the other curves gives the solid line in Figure 15. This comparison shows that the observed frequency spread matches the theory extremely well.

The model predicts that the electrostatic bursts should have a phase velocity of approximately the beam velocity. If the phase velocity is 1/20 the speed of light (corresponding to a 640 eV electron

beam), and the burst frequency is 10 kHz, then $\lambda_{\text{burst}} = 1.5$ km. This wavelength is in agreement with the observationally determined limits on λ_{burst} given in Section II. The resistive-medium instability has thus been shown to be in agreement with essentially all of the characteristics of the electrostatic bursts.

This study could also prove useful in understanding certain phenomena in regions other than the Earth's outer magnetosphere. Phenomena similar to the electrostatic bursts described in this paper have been observed in the Voyager 1 wideband data. The Voyager data were taken in the outer Saturnian magnetosphere, on the dayside of Saturn, very similar to the situation in the Earth's magnetosphere.

A report by Kennel et al. [1980] using data from the ISEE 3 spacecraft described correlated whistler mode and electron plasma oscillation bursts in the solar wind with characteristics very similar to the waves described in this report. This spacecraft is in a halo orbit around the Earth-Sun line about $235 R_E$ upstream from the earth. Because the ISEE 3 spacecraft lacked wideband instrumentation, it was not possible to obtain waveform measurements comparable to those obtained from ISEE 1. It is thus not clear if the "electron plasma oscillations" reported by Kennel et al. [1980] were below the plasma frequency or not. The interaction between the two wave modes described in this study is now regarded as a better explanation for the ISEE 3 observations than the secondary impulsive electron heating mechanism proposed by Kennel et al. [1980].

Another possible application of this work is to the study of x-ray microbursts in the auroral zone [Oliven and Gurnett, 1968]. The energetic electron precipitation (> 10 keV) causing these microbursts is usually attributed to pitch angle scattering associated with the generation of chorus. However, at high magnetic latitudes trapping and acceleration of electrons by Landau resonant interactions with whistler mode chorus could produce these electrons.

Thus, the interaction between the whistler mode chorus waves and the observed electrostatic bursts described in this study would appear to have possible relevance in a large number of space physics phenomena. Though this interaction is best understood for the Earth's outer magnetosphere, it could explain some features in other space physics data that are not presently understood.

VI. CONCLUSIONS

This study has revealed several new aspects of wave-particle interactions in the Earth's outer magnetosphere. It has described the observational characteristics of a type of electrostatic burst that is strongly associated with whistler mode chorus waves. A simple model was developed that explains these electrostatic bursts by the trapping and acceleration of electrons in Landau resonance with the electromagnetic chorus wave. This simple model is supported by a computer particle simulation of an electron interacting with a growing chorus wave which indicates that trapping should occur. By any of several mechanisms the chorus wave phase velocity could increase, accelerating any electrons trapped in Landau resonance with the chorus wave. This acceleration is in many respects similar to the traveling-wave linear particle accelerators used in high energy physics. Results from the LEPED data show a significant field-aligned electron enhancement or beam at approximately the chorus phase velocity when chorus waves and electrostatic bursts of long duration are observed.

We conclude that the resistive-medium instability can account for the generation of the electrostatic bursts by trapped electrons. This instability is valid where the beam velocity is on the order of the plasma electron thermal velocity, which is shown to be the case for the region of interest based on simultaneous plasma data. The resistive-

medium instability provides an explanation of the downshift in frequency of the bursts below the local plasma frequency. In addition, the theory predicts a relationship between the frequency spread of the bursts and the frequency downshift for the burst that is in good agreement with the observed spectrum. Overall, very strong evidence is presented that Landau interactions with whistler mode chorus is occurring and that the resistive-medium instability is the mechanism responsible for the generation of the associated electrostatic bursts.

ACKNOWLEDGEMENTS

We wish to thank Dr. Roger R. Anderson and Dr. Dennis L. Gallagher for great assistance in the analysis of ISEE data, and Dr. Louis Frank for permission to use the LEPEDea data from the ISEE 1 spacecraft.

This research was supported by NASA through grants NGL-16-001-002 and NGL-16-001-043 from NASA Headquarters and contracts NAS5-20093, NAS5-26819, and NAS5-11074 with Goddard Space Flight Center, and the Office of Naval Research. The LEPEDea data reduction from the ISEE 1 instrument was performed through contract NAS5-26257 with Goddard Space Flight Center.

APPENDIX A: DERIVATION OF RESISTIVE-MEDIUM INSTABILITY EQUATIONS

This derivation is very similar to that derived in Briggs [1964]. The derivation is made for a one-dimensional system and utilizes a dispersion relation for a weak electron beam ($n_b \ll n_e$) streaming through a plasma, where both the electron beam and the plasma ions are cold. The background plasma electrons are warm. The dispersion relation for such a system is given in Briggs [1964] as

$$\frac{\omega_{pb}^2}{(\omega - kV_0)} = K_{\parallel}(\omega, k) \quad (A1)$$

where

$$K_{\parallel}(\omega, k) = 1 - \frac{\omega_{pi}^2}{\omega^2} - \omega_{pe}^2 \int \frac{f_{oe}(v_z) dv_z}{(\omega - k v_z)^2}, \quad (A2)$$

is the longitudinal dielectric constant of the plasma in the absence of the beam, V_0 is the beam velocity, ω_{pe} and ω_{pi} are the electron and ion plasma frequencies, ω_{pb} is the plasma frequency due only to the electron beam, and f_{oe} is the electron distribution function for the warm plasma electrons.

For mathematical simplicity, a resonance distribution function for the electrons is assumed, of the form

$$f_{oe}(V_z) = \frac{V_T}{\pi} \left(\frac{1}{V_z^2 + V_T^2} \right), \quad (A3)$$

where V_T is the average longitudinal thermal velocity.

The integral in Equation A1 can be computed by taking a contour in the upper half of the complex V_z plane with the result

$$\omega_{pe} \int \frac{f_{oe}(v_z) dv_z}{(\omega - kv_z)^2} = \frac{\omega_{pe}}{(\omega - i k V_T)^2}.$$

Thus Equation A2 becomes

$$K_1(\omega, k) = 1 - \frac{\omega_{pi}^2}{\omega^2} - \frac{\omega_{pe}^2}{(\omega - i k V_T)^2}. \quad (A4)$$

An approximate solution for beam waves from Equation A1 is obtained by expanding around the beam velocity, $\omega \approx kV_0$. Equation A1 is then rewritten using the form $\omega - kV_0 = \delta\omega(k)$ where $\delta\omega \ll kV_0$. In this derivation $\delta\omega(k)$ is considered to be a small "correction" to ω caused by the presence of the beam. It should be noted that the entire imaginary component of ω , which gives the growth rate, is contained in the $\delta\omega$ term. Since $\delta\omega$ is a small correction we can perform a Taylor series expansion of Equation A1 around $\omega = kV_0$ and obtain

$$\frac{\omega^2}{\delta\omega^2} \frac{pb}{\omega^2} = k_{\parallel}(\omega = kV_0) + \delta\omega \left(\frac{\partial K_{\parallel}}{\partial \omega} \right)_{\omega=kV_0} \quad (A5)$$

Now in general, $K_{\parallel}(\omega = kV_0) = K_R + i K_I$ where the imaginary part of K_{\parallel} arises from Landau damping. Instability occurs whenever a complex $\delta\omega$ with $\text{Im}(\delta\omega) < 0$ arises from Equation A5. As described in Briggs [1964] there are two basic mechanisms that can cause instabilities. These are referred to as the reactive-medium instability and the resistive-medium instability.

The reactive-medium instability occurs if $V_0 \gg V_T$. In this case Landau damping can be neglected. This implies that K_I is vanishingly small and may be neglected in the solution of Equation A5. The solution obtained in this case is essentially the usual dispersion relation for Langmuir oscillations generated by a two-stream instability.

Of particular interest to this work is the resistive-medium instability. This instability is obtained from Equation A5 when $V_0 \approx 0(V_T)$ and $K_R > 0$. When V_0 is on the order of V_T , K_I cannot be neglected and Landau damping plays an important role in the solution of Equation A5. The novel feature in the resistive-medium instability is that it requires Landau damping to obtain wave growth. If the final term is neglected in Equation A5 we obtain (using Equation A4)

$$\begin{aligned} \frac{\omega}{\delta\omega^2} \frac{pb}{\omega^2} &= K_{\parallel}(\omega = kV_0) \\ &= 1 - \frac{\omega_{pi}^2}{\omega^2} - \frac{\omega_{pe}^2}{\omega^2 (1 - i \frac{V_T}{V_0})^2} \end{aligned}$$

which can be written

$$\delta\omega^2 = \omega_{pb}^2 \left[\frac{\omega^2(V^* - i 2 \frac{V_T}{V_o})}{\omega^*(V^* - i 2 \frac{V_T}{V_o}) - \omega_{pe}} \right], \quad (A6)$$

where $V^* = 1 - (V_T/V_o)^2$, $\omega^* = \omega^2 - \omega_{pi}^2$.

Multiplying the top and bottom by the complex conjugate one obtains

$$\delta\omega^2 = \omega_{pb}^2 [x + iy], \quad (A7)$$

$$\text{where } x = \frac{\omega^2 V^* (\omega^* V^* - \omega_{pe}^2) + 4\omega^2 (\frac{V_T}{V_o})^2 \omega^*}{(\omega^* V^* - \omega_{pe}^2)^2 + 4(\omega^*)^2 (\frac{V_T}{V_o})^2} \quad (A9)$$

$$\text{and } y = \frac{2\omega^2 (\frac{V_T}{V_o}) \omega_{pe}^2}{(\omega^* V^* - \omega_{pe}^2)^2 + 4(\omega^*)^2 (\frac{V_T}{V_o})^2} \quad (A9)$$

Thus $\delta\omega$ may be found by taking the complex square root of

$\omega_{pb}^2 [x + iy]$, so that

$$\delta\omega = \pm \omega_{pb} [x + iy]^{1/2} \quad (A10)$$

will be the solution for the resistive-medium instability.

REFERENCES

- Anderson, R. R., G. K. Parks, T. E. Eastman, D. A. Gurnett, and L. A. Frank, Plasma waves associated with energetic particles streaming into the solar wind from the Earth's bow shock, J. Geophys. Res., 86, 4493, 1981.
- Brice, N., Fundamentals of very low frequency emission generation mechanisms, J. Geophys. Res., 69, 4515, 1964.
- Briggs, R. J., Electron-Stream Interaction With Plasmas, Research Monograph No. 29, M.I.T. Press, Cambridge, Massachusetts, 1964.
- Burtis, W. J., and R. A. Helliwell, Banded chorus - A new type of VLF radiation observed in the magnetosphere by OGO 1 and OGO 3, J. Geophys. Res., 74, 3002, 1969.
- Burton, R. K., and R. E. Holzer, The origin and propagation of chorus in the outer magnetosphere, J. Geophys. Res., 79, 1014, 1974.
- Dowden, R. L., Doppler-shifted cyclotron radiation from electrons: A theory of very low frequency emissions from the exosphere, J. Geophys. Res., 67, 1745, 1962.

Eastman, T. E., and L. A. Frank, Observations of high-speed plasma flow near the Earth's magnetopause: Evidence for reconnection?, J. Geophys. Res., 87, 2187, 1982.

Frank, L. A., D. M. Yeager, H. D. Owens, K. L. Ackerson, and M. R. English, Quadrispherical LEPEDAS for ISEE's-1 and -2 plasma wave measurements, IEEE Trans. Geosci. Electron., GE-16, 221, 1978a.

Frank, L. A., K. L. Ackerson, R. J. DeCoster, and B. G. Burek, Three-dimensional plasma measurements within the earth's magnetosphere, Space Sci. Rev., 22, 739, 1978b.

Gurnett, D. A., and L. A. Frank, Ion acoustic waves in the solar wind, J. Geophys. Res., 83, 58, 1978.

Gurnett, D. A., and R. R. Shaw, Electromagnetic radiation trapped in the magnetosphere above the plasma frequency, J. Geophys. Res., 78, 8136, 1973.

Gurnett, D. A., F. L. Scarf, R. W. Fredricks, and E. J. Smith, The ISEE-1 and ISEE-2 plasma wave investigation, IEEE Trans. Geosci. Electron., GE-16, 225, 1978.

Helliwell, R. A., Whistlers and Related Ionospheric Phenomena, Stanford University Press, 1965.

Helliwell, R. A., A theory of discrete VLF emissions from the magnetosphere, J. Geophys. Res., 72, 4773, 1967.

Inan, U. S., and S. Tkalcevic, Nonlinear equations of motion for landau resonance interactions with a whistler mode wave, J. Geophys. Res., 87, 2363, 1982.

Kennel, C. F., and H. E. Petschek, Limit on stably trapped particle fluxes, J. Geophys. Res., 71, 1, 1966.

Kennel, C. F., F. L. Scarf, F. V. Coroniti, R. W. Fredricks, D. A. Gurnett, and E. J. Smith, Correlated whistler and electron plasma oscillation bursts detected on ISEE 3, Geophys. Res. Lett., 7, 129, 1980.

Kennel, C. F., and R. M. Thorne, Unstable growth of unducted whistlers propagating at an angle to the geomagnetic field, J. Geophys. Res., 72, 871, 1967.

Krall, N. A., and A. W. Trivelpiece, Principles of Plasma Physics, McGraw-Hill, 1973.

Mikhailovskii, A. B., Theory of Plasma Instabilities (Volume 1: Instabilities of a Homogeneous Plasma), Consultants Bureau, New York - London, 1974.

Nunn, D., Wave particle interaction in electrostatic waves in an inhomogeneous medium, J. Plasma Phys., 6, 291, 1971.

Nunn, D., The sideband instability of electrostatic waves in an inhomogeneous medium, Planet. Space Sci., 21, 67, 1973.

Oliven, M. N., and D. A. Gurnett, Microburst phenomena 3. An association between microbursts and VLF chorus, J. Geophys. Res., 73, 2355, 1968.

Reinleitner, L. A., Electrostatic bursts generated by electrons trapped in whistler mode chorus wave fields, Ph.D. Dissertation, The University of Iowa, 1982.

Reinleitner, L. A., D. A. Gurnett, and D. L. Gallagher, Chorus-related electrostatic bursts in the Earth's outer magnetosphere, Nature, 295, 46, 1982.

Rosenberg, T. J., R. A. Helliwell, and J. P. Katsufakis, Electron precipitation associated with discrete very-low-frequency emissions, J. Geophys. Res., 76, 8445, 1971.

Russell, C. T., The ISEE 1 and 2 fluxgate magnetometers, IEEE Trans. Geosci. Electron., GE-16, 239, 1978.

Stix, T. H., The Theory of Plasma Waves, McGraw-Hill, New York, N.Y., 1962.

Tkalcevic, S., Nonlinear Longitudinal Resonance Interaction of Energetic Charged Particles and VLF Waves in the Magnetosphere, Ph.D. Dissertation, Stanford University, 1982.

Van Allen, J. A., Dynamics, composition and origin of the geomagnetically-trapped corpuscular radiation, Transactions of the International Astronomical Union, 11B, 99, 1962.

FIGURE CAPTIONS

- Figure 1 ISEE 1 frequency-time wideband data illustrating the main characteristics of the electrostatic bursts and their relationship to whistler mode chorus waves. In this case, the electrostatic bursts are correlated to the discrete "hooks" in the chorus band. The bursts have a much higher frequency range than the chorus and a wider frequency spread. The plasma frequency and the electron gyrofrequency are indicated at the right. The lower edge of the continuum radiation is used to determine the plasma frequency. The time interval covered is one minute.
- Figure 2 ISEE 1 frequency-time wideband data illustrating the main characteristics of the long time duration electrostatic bursts when they are correlated with an intensification of the chorus band, but no single discrete chorus feature. The time interval covered is one minute.
- Figure 3 An example of the electric field spectral density versus frequency taken at both ISEE 1 and ISEE 2 during a long electrostatic burst which was observed at both spacecraft. The electric field spectral density is corrected

for the different electric dipole antenna lengths on the two spacecraft. The fact that both the chorus and the electrostatic bursts have almost identical spectral densities indicates that the wavelengths of both waves are significantly longer than either spacecraft antenna.

Figure 4

Rapid sample electric field data for the 10 kHz channel of the multichannel spectrum analyzer showing the longitudinal nature of the electrostatic burst. The burst, centered near 10 kHz, is sampled at 32 samples per second and is plotted against the spin angle ϕ of the spacecraft. As indicated, the maximum electric field strength occurs when the dipole antenna was oriented along the projection of the magnetic field onto the spin plane of the spacecraft. This indicates that the burst is polarized with the electric field aligned along the ambient magnetic field.

Figure 5

The lower panel shows the oscilloscope waveform pattern taken from the very short burst indicated in the frequency-time spectrogram. The low frequency signal in the bottom of the lower panel is the chorus waveform while the high frequency signal bursts at the top of the lower panel are the electrostatic bursts. The amplitude of the electrostatic bursts is modulated by the chorus waveform. It should be noted that the duration of the lower panel is only eight milliseconds.

Figure 6 Four examples of oscilloscope waveform are shown. In all cases the top trace is that of the chorus while the bottom trace is that of the electrostatic burst. The two left examples (A and B) are taken from a short burst correlated with a chorus hook (B) being an expansion of part of (A). The amplitude modulation of the bursts by the chorus waveform is very evident. The two right examples (C and D) are from a long burst just a few minutes earlier. These again have different time scales, (D) being an expansion of (C). In this case the amplitude modulation of the electrostatic noise is not closely associated with the chorus waveform.

Figure 7 Illustration of the model proposed for whistler mode electron trapping and burst generation. The top panel shows how a wave propagating at an angle to \vec{B}_0 produces an \vec{E}_\parallel (parallel) field, while the middle panel illustrates how an electron moving along the magnetic field line sees an effective potential associated with \vec{E}_\parallel and can be trapped at the whistler mode phase velocity. The lower panel shows how these trapped electrons can generate electrostatic emissions modulated at the chorus phase velocity.

Figure 8 Three cases of particle trapping produced by computer modeling for different wave vector angles (θ) to the

ambient magnetic field. Z-phase is the phase relation between the electron and the whistler mode wave. Trapping occurs when the phase variation is bounded. In the model, the electric field intensity of the whistler mode wave increases linearly with time, and so the abscissa is marked as both time and E_0 .

Figure 9 Illustration of a possible mechanism for producing a distinct electron beam in the electron distribution function. In this suggested scenerio, the chorus phase velocity increases and the trapped electrons are accelerated to higher velocities. The velocity increase has been exaggerated for clarity.

Figure 10 E- ϕ spectrogram for day 222 of 1979 from the LEPDEA data. The beam-like features indicated by the arrows are the magnetic field-aligned electron enhancements, which occur simultaneously with the long electrostatic burst. This figure is a black and white version of the color plate used in the paper submitted to J. Geophys. Res.

Figure 11 A composite figure showing the correspondence between a very long electrostatic burst and the field-aligned electron beams shown in the LEPDEA data. The upper panels are frequency-time wideband data from ISEE 1 showing a 2.5-minute burst with the start time marked with an S and

the end time marked with a T. The lower panels are a time mosaic of detectors 2E and 6E from the E - ϕ spectrograms for approximately the same ten-minute interval. Both time and energy increase along the ordinate of each E - ϕ spectrogram. The ϕ -independent enhancements below the beam energy at about 100 eV are associated with photoelectrons. It is clear that the field-aligned enhancement at ≈ 400 eV is strongest during the burst period, although it also persists at lower intensities for several minutes after the termination of the burst.

Figure 12 Perspective plot of the electron distribution function from the LEPDEA data for day 222 of 1979. The two field-aligned electron enhancements are indicated.

Figure 13 Graph of the imaginary component of ω versus the real component of ω for the resistive-medium instability with several different values of V_0/V_T . The downshift in the frequency of maximum growth rate below the plasma frequency (ω_{pe}) for progressively lower values of V_0/V_T is clearly evident. The dotted lines are used to calculate the points labeled "theory" in Figure 15.

Figure 14 Graph of the frequency of the maximum growth rate of the resistive-medium instability versus V_0/V_T . This plot

shows that the frequency of maximum growth rate is shifted well below the plasma frequency for small values for V_0/V_T .

Figure 15 Plot of observed points in the wideband data showing the frequency bandwidth spread versus the downshift in the burst frequency below the plasma frequency. The theoretical points were computed using the graph shown in Figure 13.

B-682-640

ISEE-1 NOVEMBER 28, 1980 DAY 333
R = 9.33 R_E MAG LAT = 17.8° MLT = 6.5 HRS

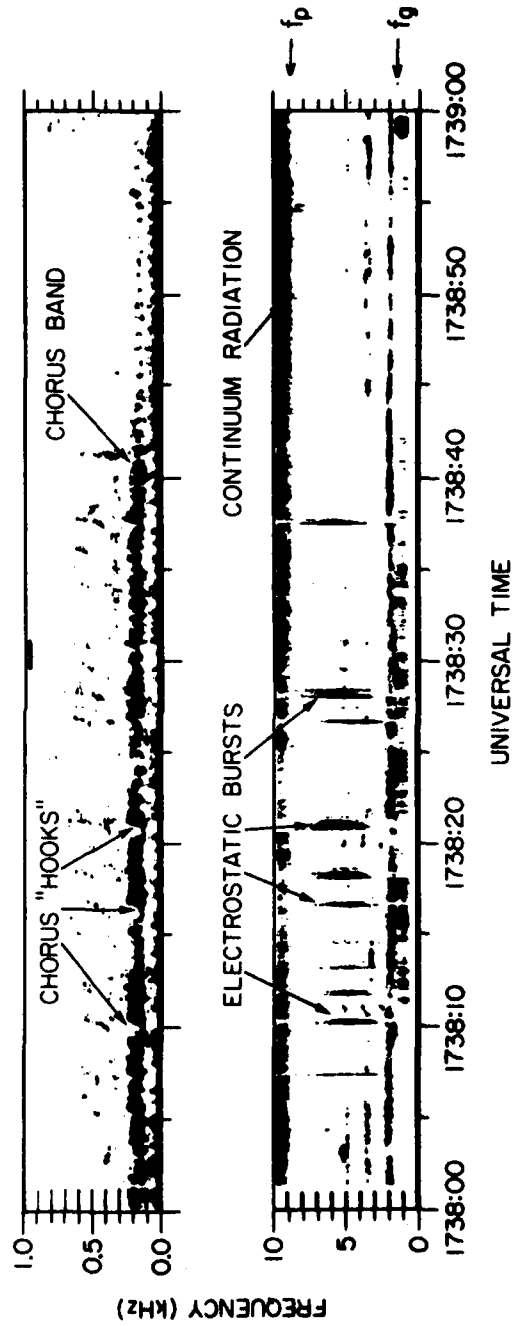


Figure 1

A-G81-1085

ISEE 1 SEPTEMBER 19, 1978 DAY 262
R = 11.8 R_E MAG LAT = -4.5° MLT = 14.4 HRS

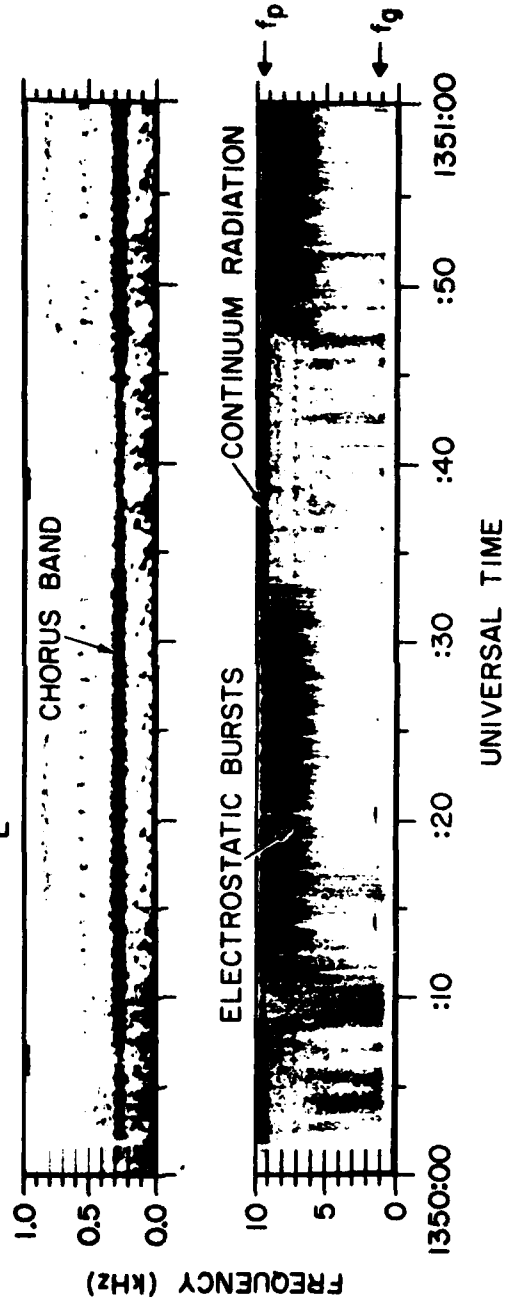


Figure 2

A-681-1055

ISEE 1 & 2 NOVEMBER 29, 1977

MAG LAT = 18.8° MLT = 10.3 HRS

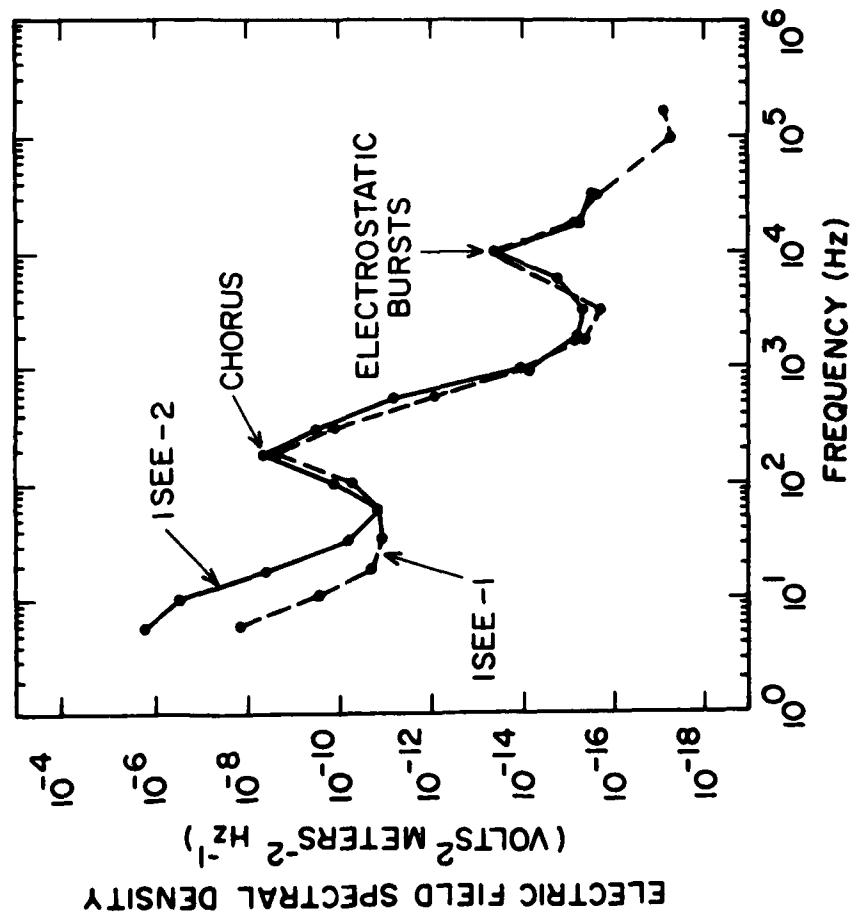
R = 10.3 R_E R = 672 km 1551:15-1551:25UT.

Figure 3

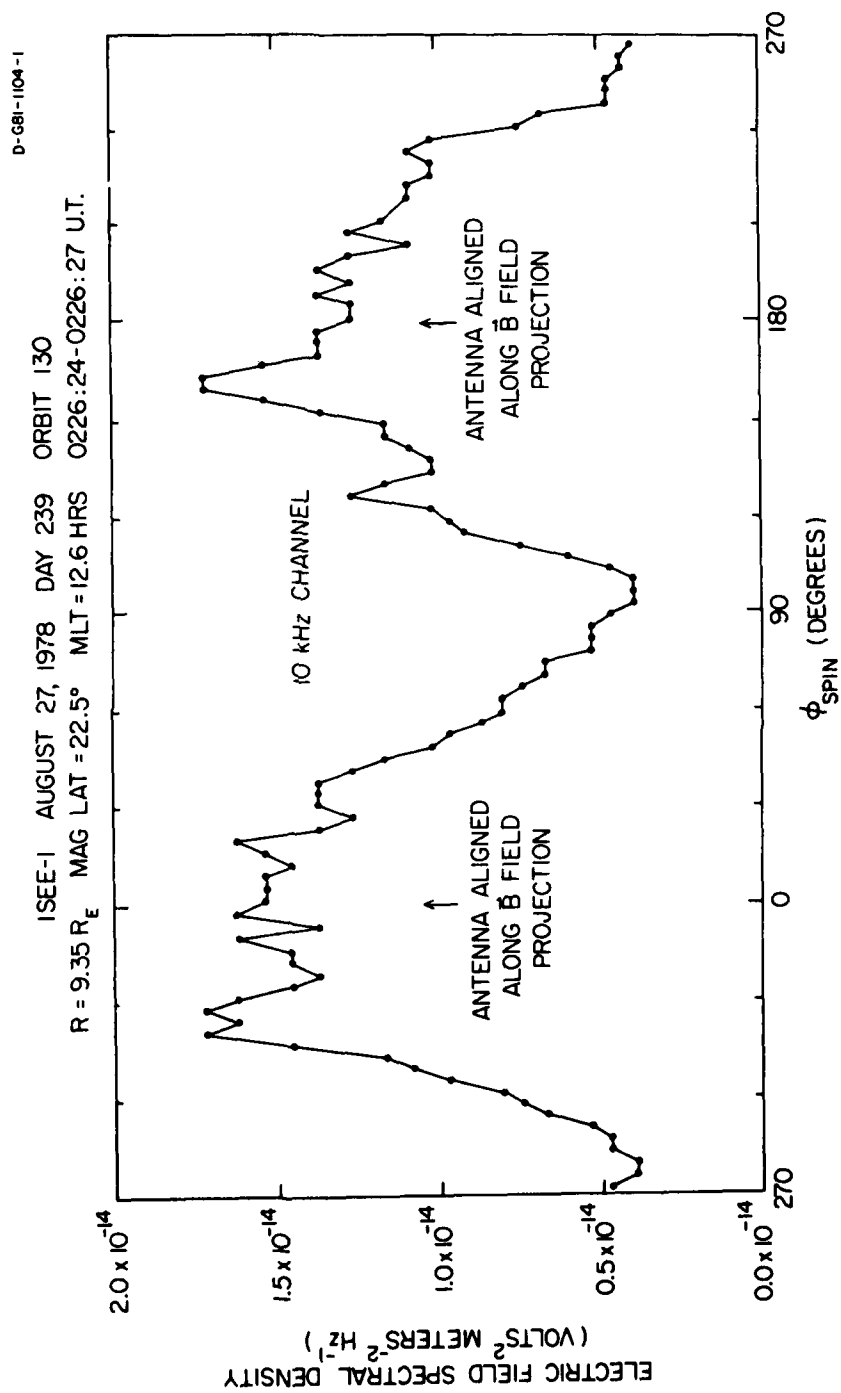


Figure 4

C-681-431-3

ISEE-1 NOVEMBER 5, 1977 DAY 309 ORBIT 6
 R = 11.04 R_E MAG LAT = 21.1° MLT = 11.6 HRS

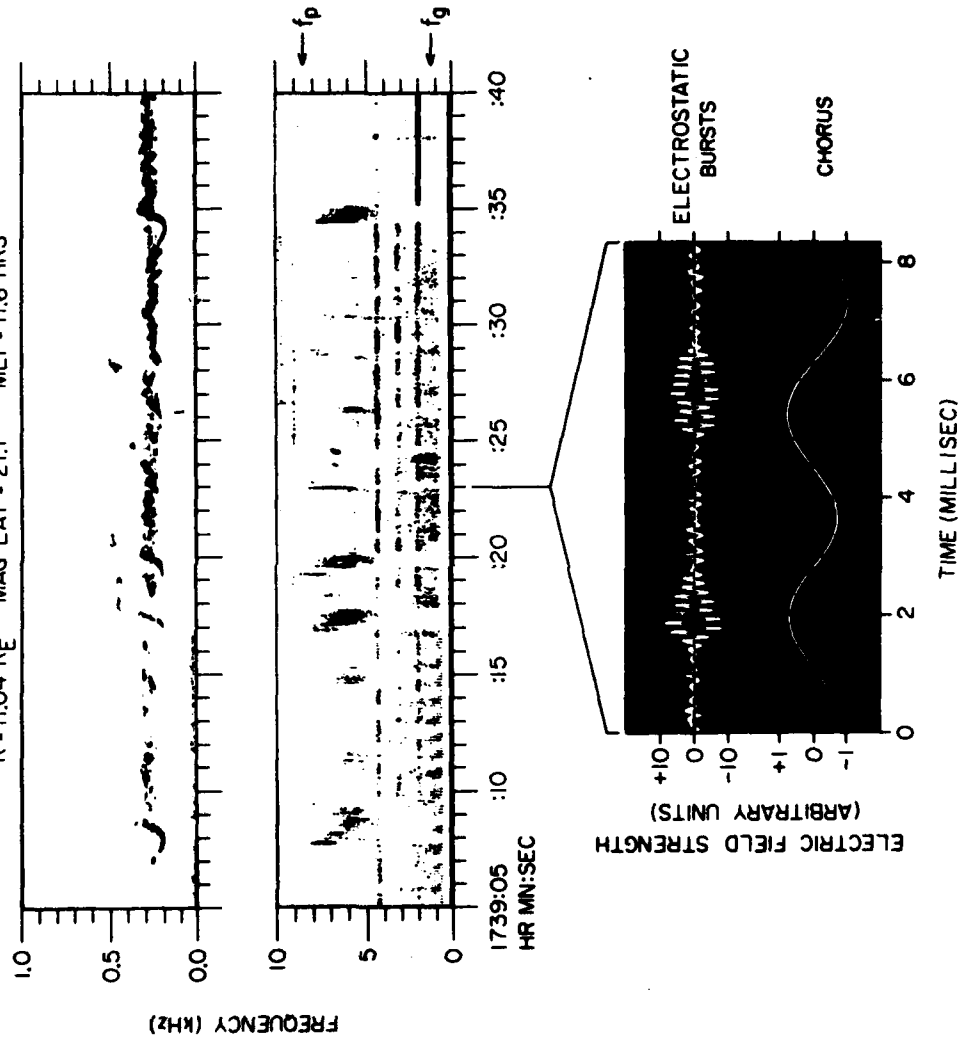
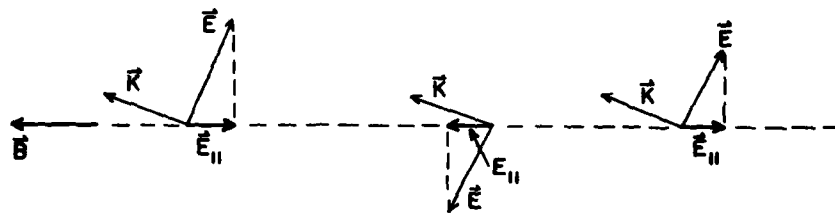
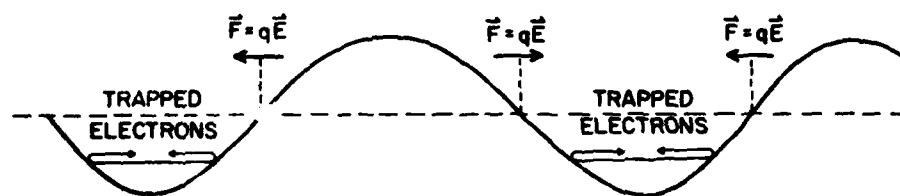


Figure 5

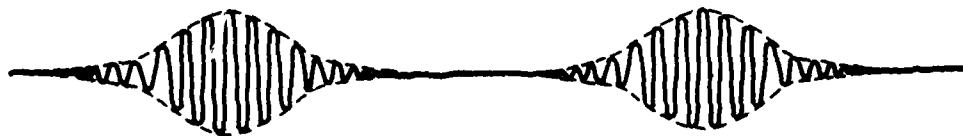
B-681-1086



CHORUS WAVE COMPONENTS



EFFECTIVE POTENTIAL



ELECTROSTATIC BURSTS

Figure 7

C-682-520

ISEE-1 NOVEMBER 29, 1977 DAY 333
R = 10.6 R_E MAG LAT = 19.3° MLT = 10.2 HRS

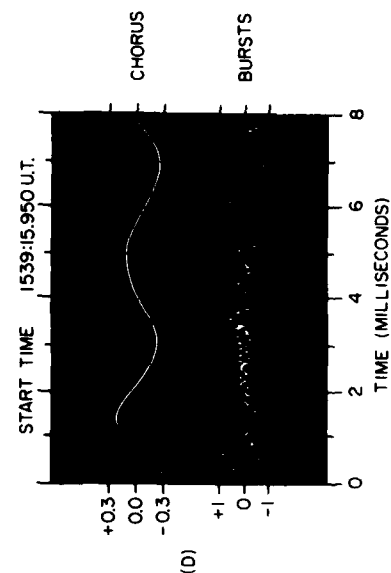
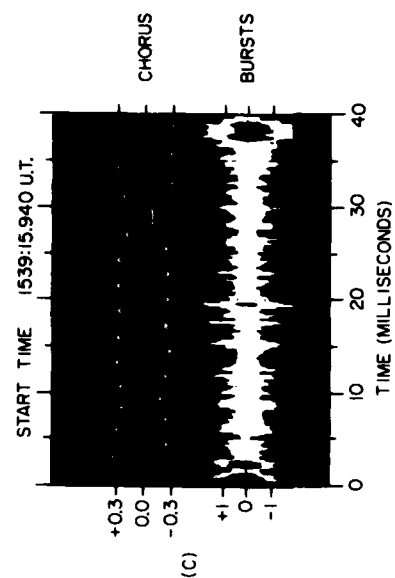
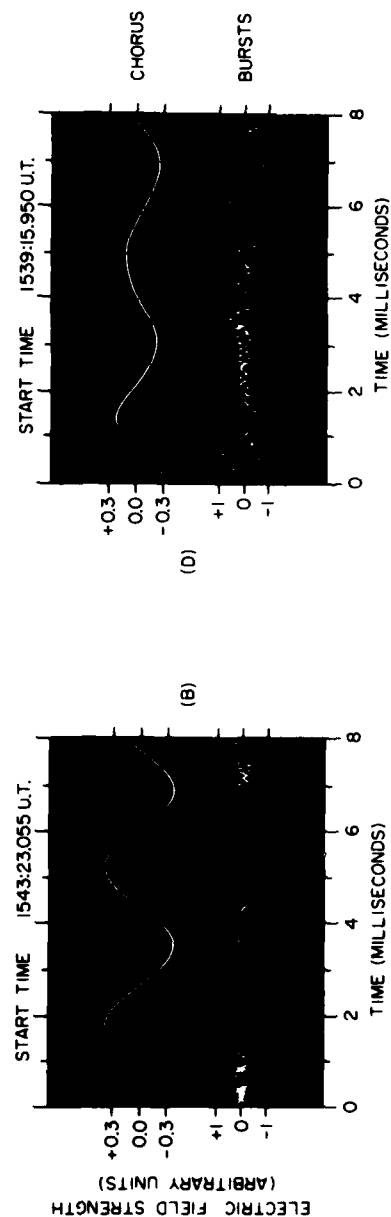
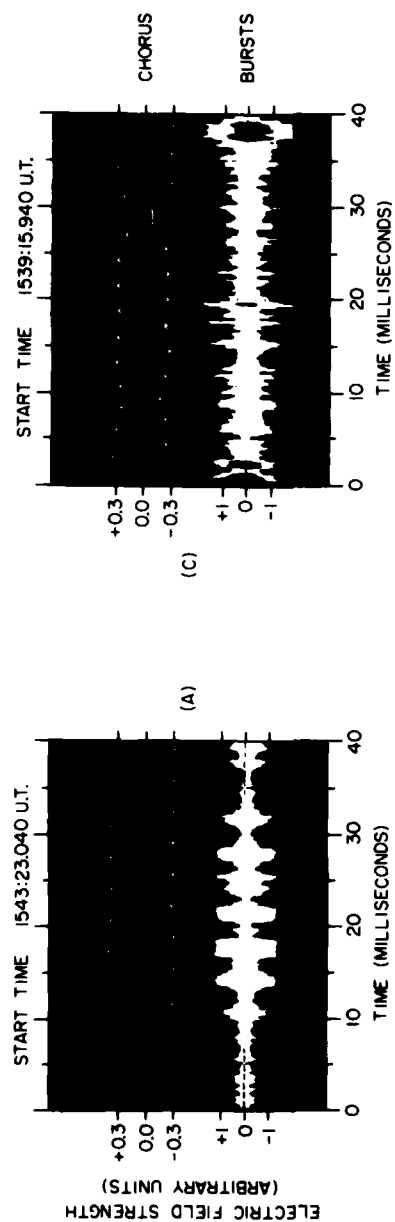


Figure 6

C-682-523-1

PARTICLE TRAPPING FROM COMPUTER MODEL

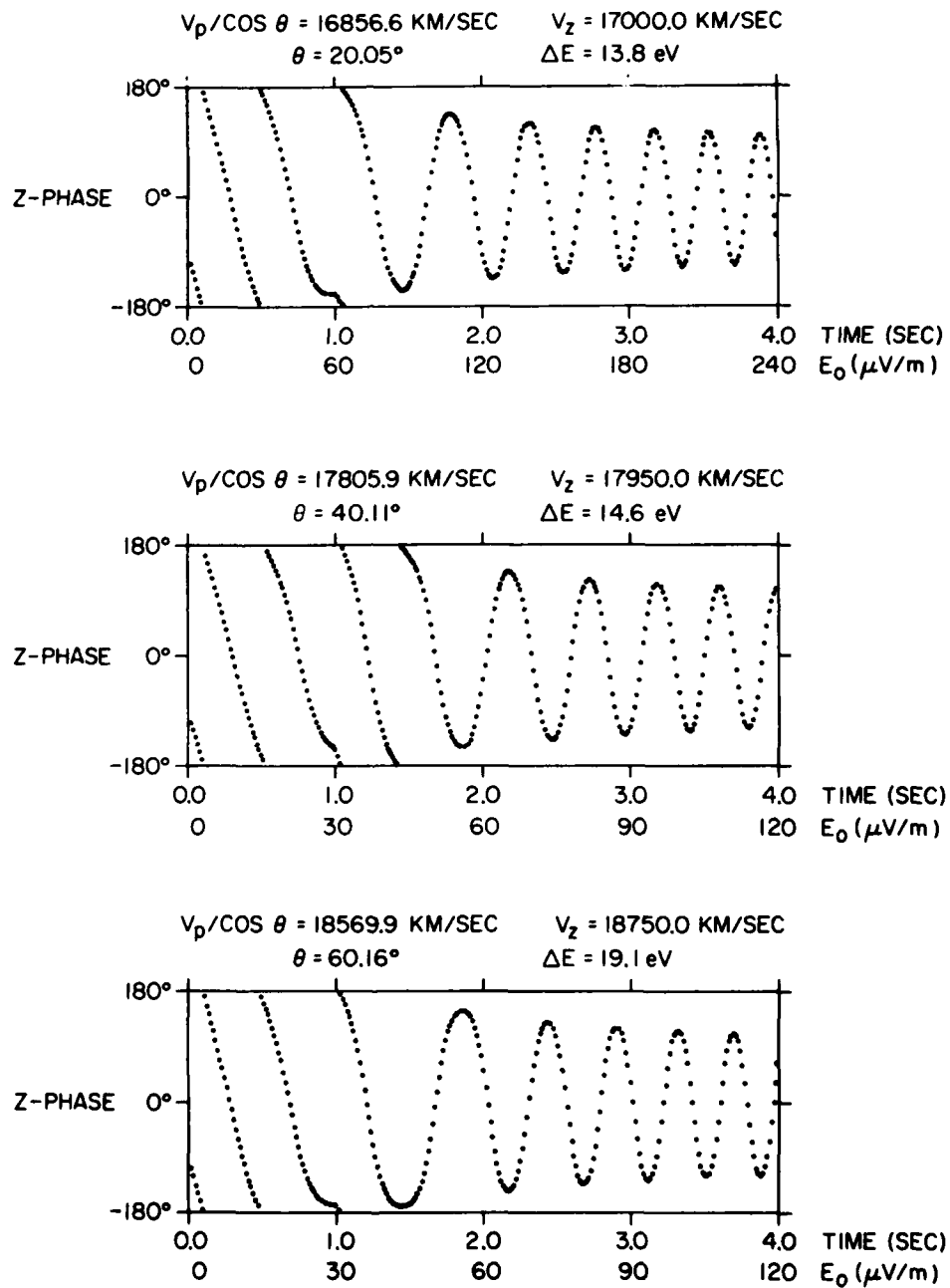
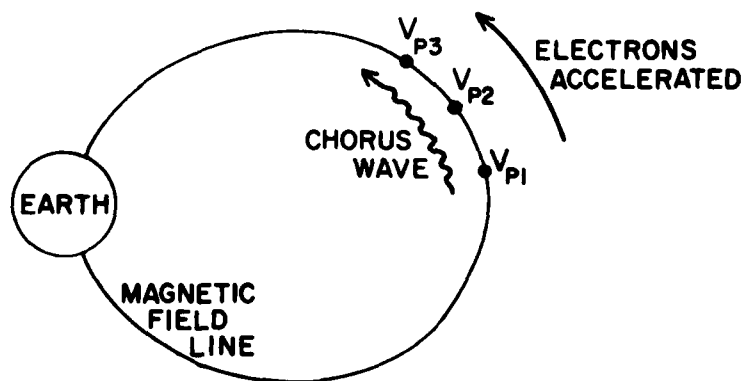
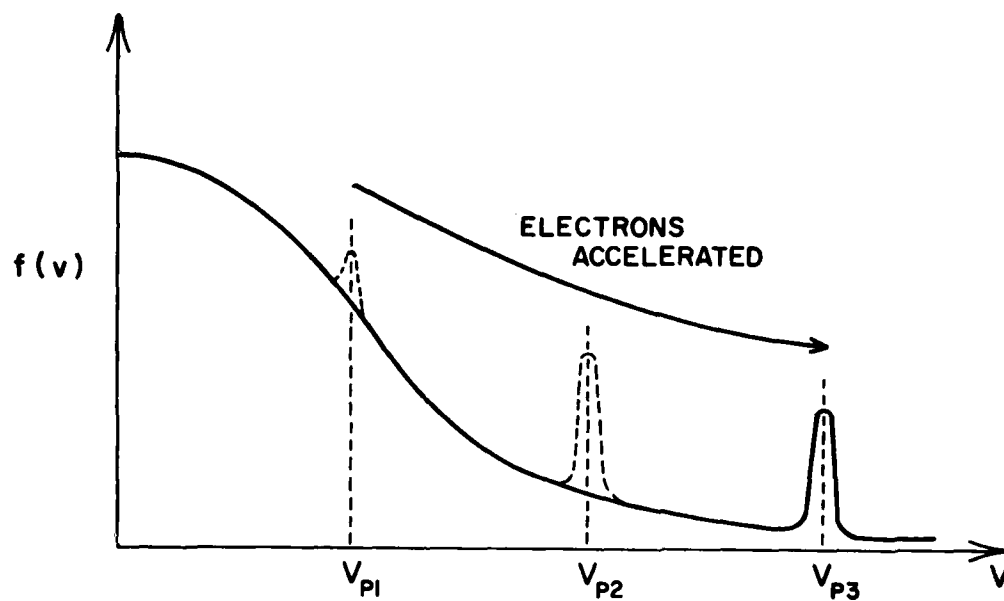


Figure 8

A-G81-1097



V_{PHASE} INCREASE \Rightarrow ACCELERATION OF TRAPPED ELECTRONS

Figure 9

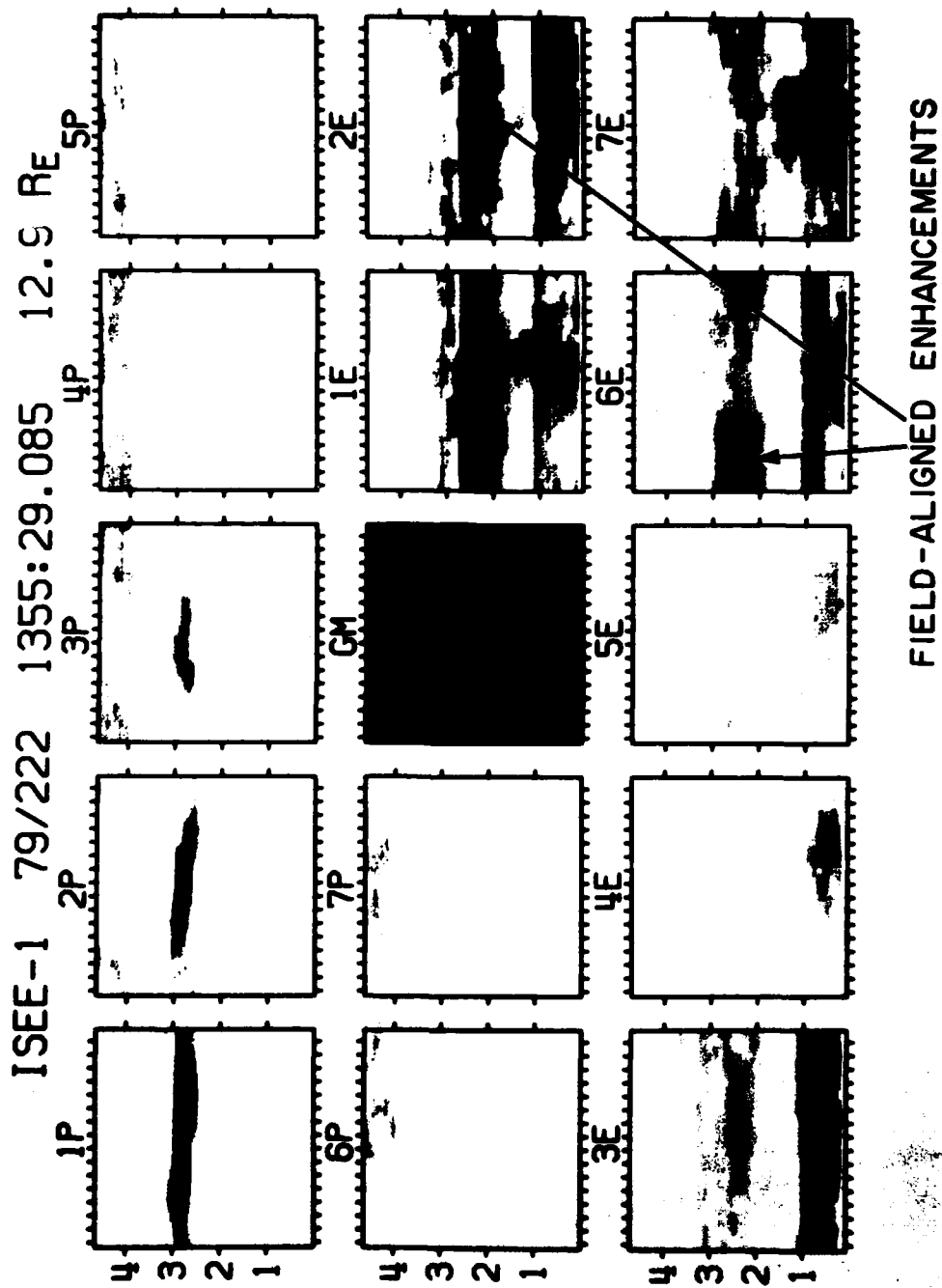


Figure 10

FREQUENCY (KHZ)

BURST START	BURST END	S	ELECTROSTATIC	T	CONTINUUM RADIATION
1	2	3	4	5	6
7	8	9	10	11	12
13	14	15	16	17	18
19	20	21	22	23	24
25	26	27	28	29	30
31	32	33	34	35	36
37	38	39	40	41	42
43	44	45	46	47	48
49	50	51	52	53	54
55	56	57	58	59	60
61	62	63	64	65	66
67	68	69	70	71	72
73	74	75	76	77	78
79	80	81	82	83	84
85	86	87	88	89	90
91	92	93	94	95	96
97	98	99	100	101	102
103	104	105	106	107	108
109	110	111	112	113	114
115	116	117	118	119	120
121	122	123	124	125	126
127	128	129	130	131	132
133	134	135	136	137	138
139	140	141	142	143	144
145	146	147	148	149	150
151	152	153	154	155	156
157	158	159	160	161	162
163	164	165	166	167	168
169	170	171	172	173	174
175	176	177	178	179	180
181	182	183	184	185	186
187	188	189	190	191	192
193	194	195	196	197	198
199	200	201	202	203	204
205	206	207	208	209	210
211	212	213	214	215	216
217	218	219	220	221	222
223	224	225	226	227	228
229	230	231	232	233	234
235	236	237	238	239	240
241	242	243	244	245	246
247	248	249	250	251	252
253	254	255	256	257	258
259	260	261	262	263	264
265	266	267	268	269	270
271	272	273	274	275	276
277	278	279	280	281	282
283	284	285	286	287	288
289	290	291	292	293	294
295	296	297	298	299	300
301	302	303	304	305	306
307	308	309	310	311	312
313	314	315	316	317	318
319	320	321	322	323	324
325	326	327	328	329	330
331	332	333	334	335	336
337	338	339	340	341	342
343	344	345	346	347	348
349	350	351	352	353	354
355	356	357	358	359	360
361	362	363	364	365	366
367	368	369	370	371	372
373	374	375	376	377	378
379	380	381	382	383	384
385	386	387	388	389	390
391	392	393	394	395	396
397	398	399	400	401	402
403	404	405	406	40	

UNIVERSAL TIME

LOG₁₀ ENERGY (eV)

DETECTOR 2E

2353:36 U.T.

2355:44 U.T.

2357:52 U.T.


0000:00 U.T.

0002:08 U.T.

START TIMES

LOG₁₀ ENERGY (eV)

A schematic diagram of a beam under tension. A horizontal rectangular beam is shown with a jagged, irregular left end and a smooth right end. A double-headed vertical arrow labeled 'T' is positioned above the beam, indicating tension. The word '"BEAM"' is written inside the beam, oriented vertically. To the right of the beam, the text '300' is written vertically.



DETECTOR 6E

ISSE-1 LEPEDEA ELECTRON E -- ϕ SPECTROGRAMS 80/263--4

Figure 11

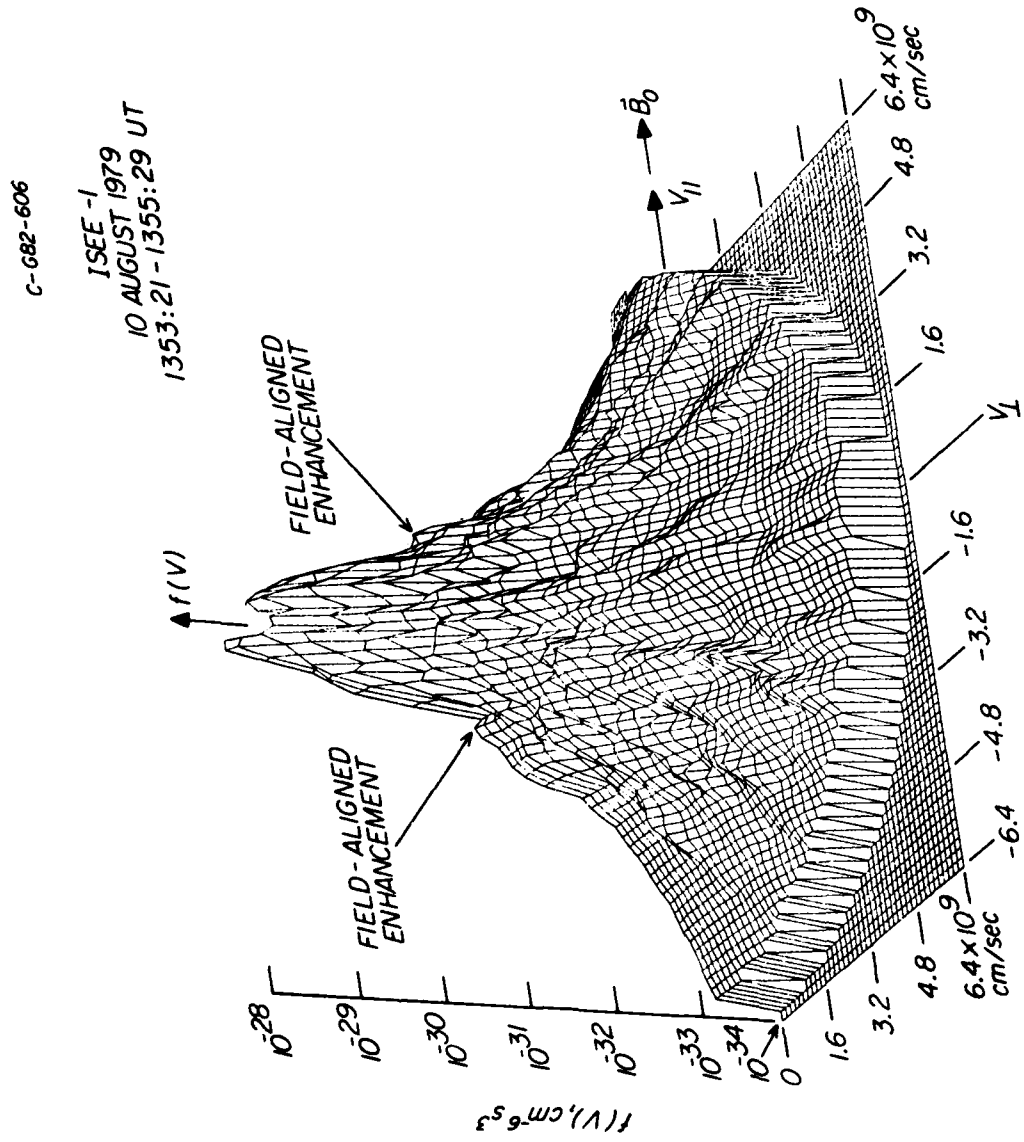


Figure 12

A-G82-506

Im(ω) VERSUS Re(ω) FOR THE
RESISTIVE-MEDIUM INSTABILITY

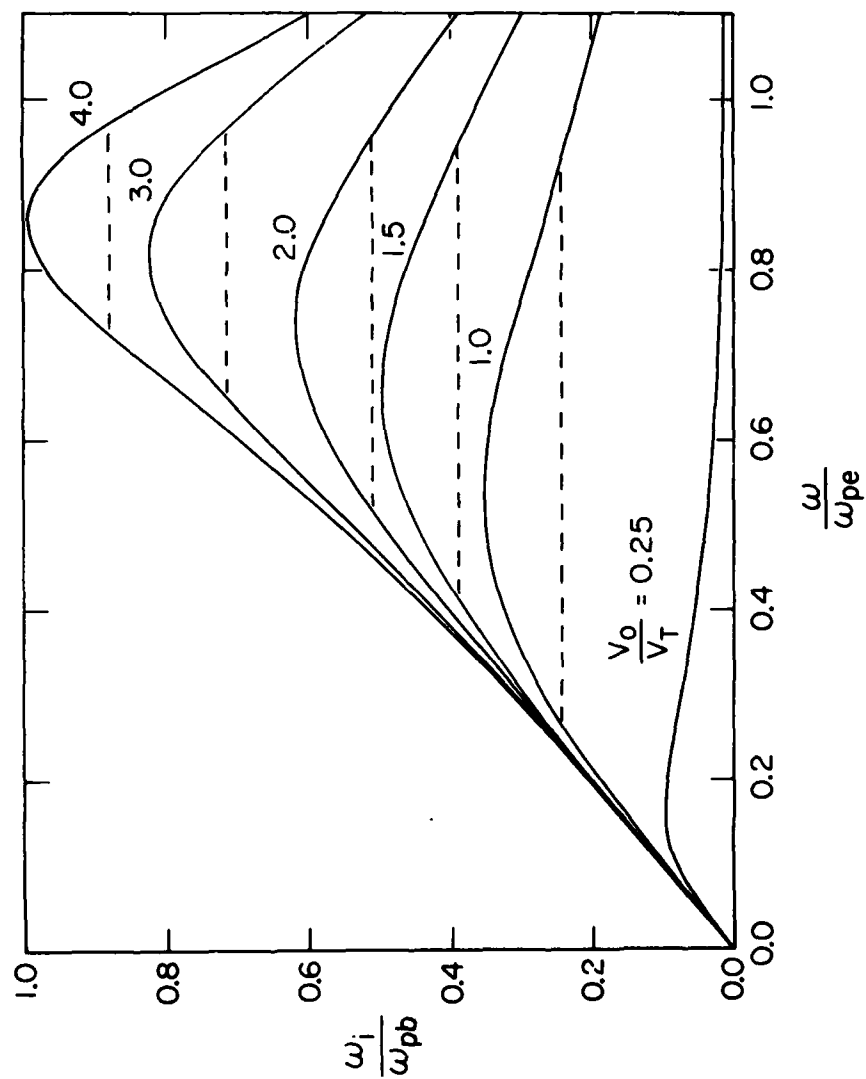


Figure 13

A-G82-445

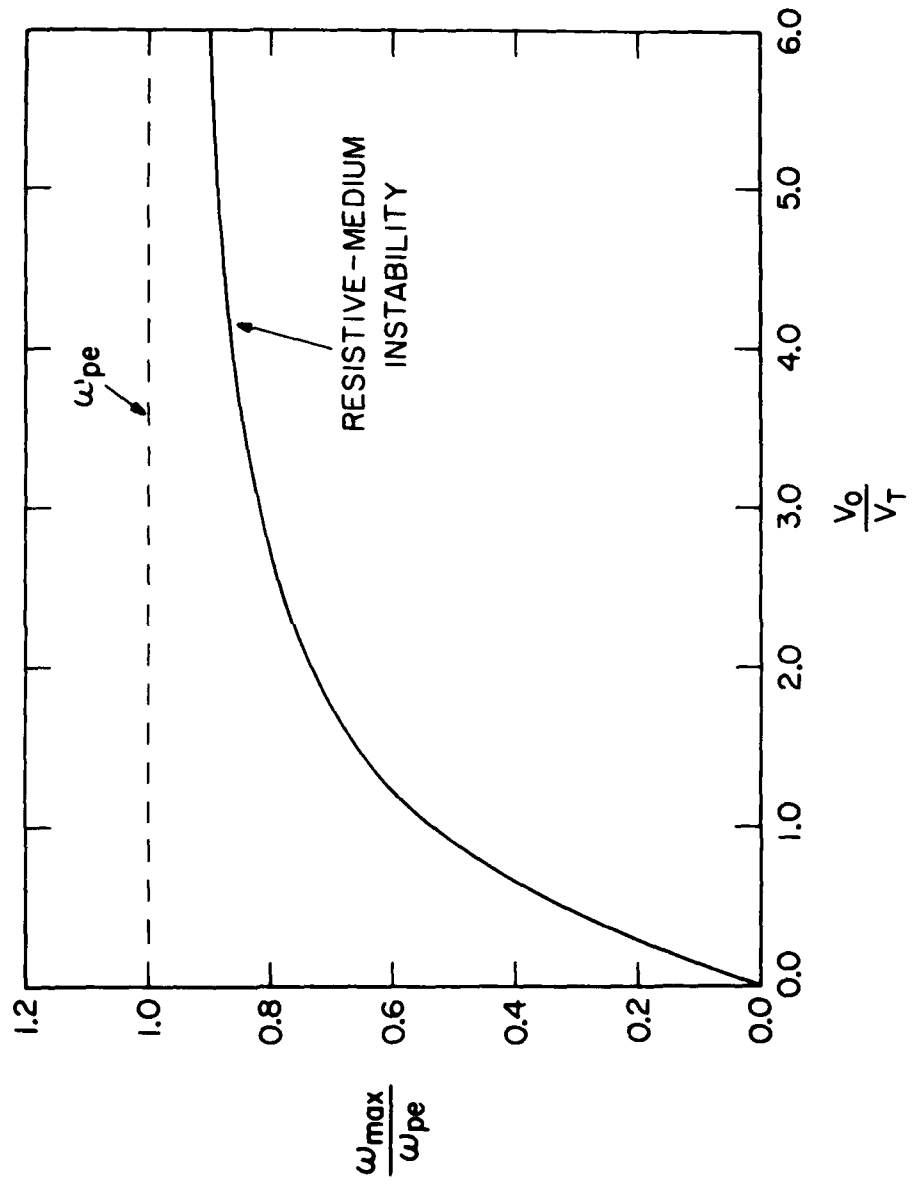
FREQUENCY OF MAXIMUM GROWTH (ω_{\max})
VERSUS BEAM VELOCITY/ELECTRON TEMP.

Figure 14

A-G82-526

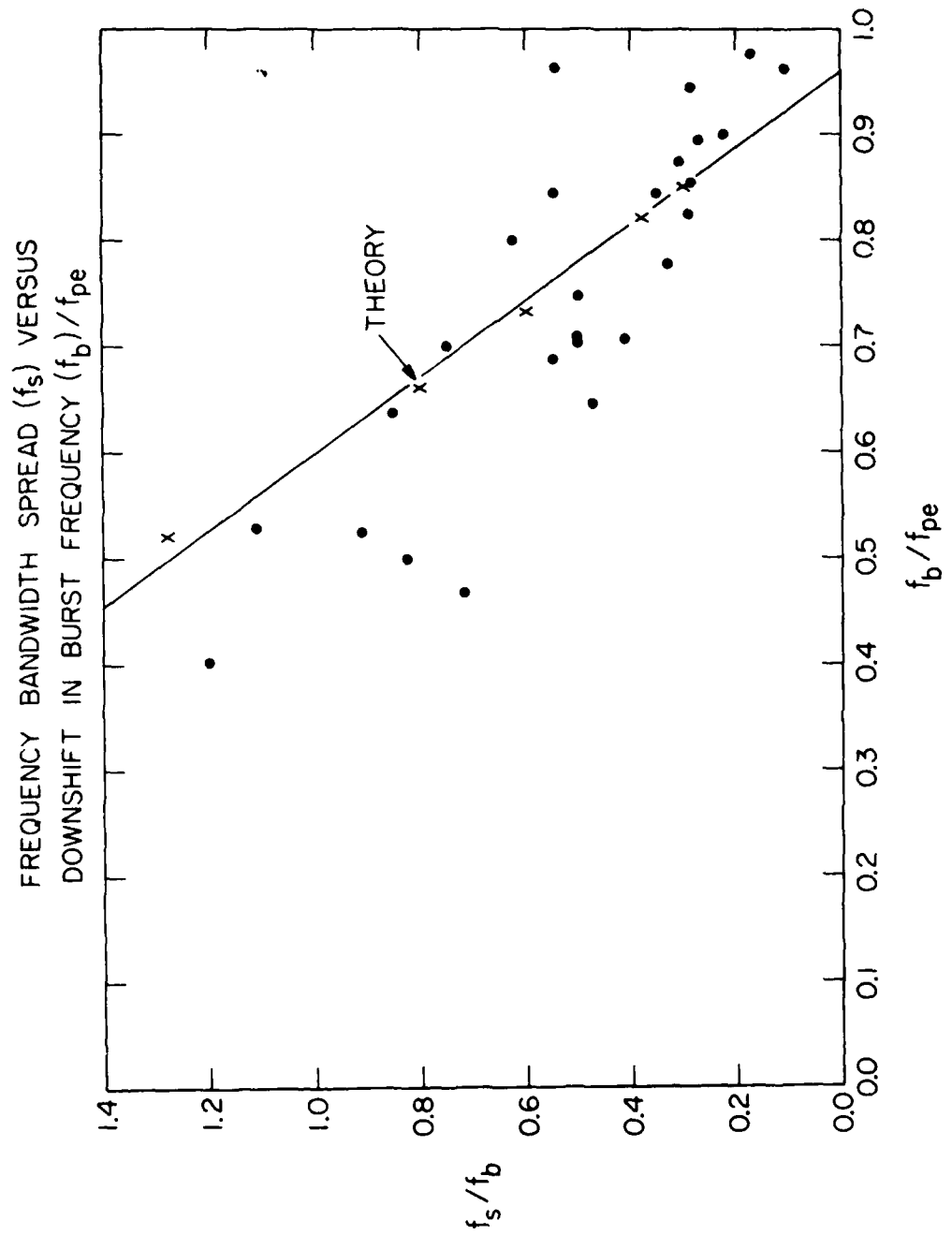


Figure 15

DATE
ILME